

ORGANISATION EUROPÉENNE POUR LA RECHERCHE NUCLÉAIRE
EUROPEAN ORGANIZATION FOR NUCLEAR RESEARCH

Laboratoire Européen pour La Physique des Particules
European Laboratory for Particle Physics

LHC CIVIL ENGINEERING CONSULTANCY SERVICES

PACKAGE 02

ADDITIONAL LABORATORY TESTS INTERPRETATIVE REPORT

DOCUMENT 11/REVISION 3

MARCH 1998



DOCUMENT CONTROL SHEET

GIBB-SGI-GEOCONSULT JOINT VENTURE

PROJECT: LHC Civil Engineering Consultancy Package 02 **JOB NO.** 96107

TITLE: Additional Laboratory Tests
Interpretative Report

ISSUE	DATE
ISSUED FOR COMMENT	September 1997
ORIGINAL	September 1997
REVISION 2	November 1997
REVISION 3	March 1998
REVISION	

This report, and information or advice which it contains, is provided by the Joint Venture in performance of Joint Venture's duties and liabilities under its contract with CERN. Any advice, opinions, or recommendations within this report should be read and relied upon only in the context of the report as a whole. The contents of the report do not, in any way, purport to include any manner of legal advice or opinion. This report is prepared in accordance with the terms and conditions of the Joint Venture's contract with CERN. Regard should be had to those terms and conditions when considering and/or placing any reliance on this report. CERN may release this report to any party having an interest or potential interest in the project. Save therefore, the release by CERN of this report is subject to prior written agreement by the Joint Venture, upon such terms and conditions as shall be agreed upon.

Copies to:

Copy	1	2	3	4	5
Holder	GIBB	Geoconsult	Prof. Descoeudres	SGI	CERN
Copy	6	7	8	9	10
Holder	CERN	CERN	CERN	CERN	GIBB

ADDITIONAL LABORATORY TESTS INTERPRETATIVE REPORT

CONTENTS

Chapter	Description	Page
1	INTRODUCTION	1-1
	1.1 Scope of work	1-1
2	EFFECTIVE STRENGTH TESTS	2-1
	2.1 Stress path testing	2-1
	2.2 Overview of results	2-1
	2.3 Effective Strength Tests - Conclusions	2-3
3	TRIAXIAL CREEP TESTS	3-1
	3.1 Introduction	3-1
	3.2 Applied loading	3-1
	3.3 Overview of results	3-1
	3.4 Triaxial Creep Tests - Conclusions	3-3
4	TRIAXIAL SWELLING TESTS	4-1
	4.1 Introduction	4-1
	4.2 Applied loading	4-1
	4.3 Overview of results	4-1
	4.4 Triaxial Swelling Tests - Conclusions	4-2
5	MINERALOGICAL ANALYSES	5-1
	5.1 Introduction	5-1
	5.2 Correlations of Mineralogy with Swelling Index Tests	5-2
	5.3 Mineralogical Analyses - Conclusions	5-3
6	ONE DIMENSIONAL SWELLING TESTS	6-1
	6.1 Introduction	6-1
	6.2 Results - Maximum Axial Swelling Stress and Axial Swelling Strain Tests	6-1

6.3	Results - Axial Swelling Stress as a Function of Swelling Strain Tests	6-2
6.4	Application of Results in Design	6-3
6.4.1	Application of One-Dimensional Test Results	6-3
6.4.2	Appropriate Design Methods	6-4
6.5	One Dimensional Swelling Tests - Conclusions and Recommendations	6-5
7	CONCLUDING REMARKS	7-1
8	REFERENCES	8-1

LIST OF FIGURES

FIGURE No.	TITLE
2.1	a) Calculated in situ stress paths and b) idealised triaxial representations
2.2	Results from triaxial strength tests
2.3	Deviator stress versus axial strain plots from triaxial strength tests
3.1a	Marl sample 8139: Axial deformation versus square root of time
3.1b	Marl sample 8139: Axial deformation versus logarithm of time
3.1c	Marl sample 8139: Axial deformation versus logarithm of time (detail)
3.2a	Marl sample 8159: Axial deformation versus square root of time
3.2b	Marl sample 8159: Axial deformation versus logarithm of time
3.2c	Marl sample 8159: Axial deformation versus logarithm of time (detail)
3.3a	Marl grumeleuse sample 8143: Axial deformation versus square root of time
3.3b	Marl grumeleuse sample 8143: Axial deformation versus logarithm of time
3.3c	Marl grumeleuse sample 8143: Axial deformation versus logarithm of time (detail)
3.4a	Marl grumeleuse sample 8274: Axial deformation versus square root of time
3.4b	Marl grumeleuse sample 8274: Axial deformation versus logarithm of time
3.4c	Marl grumeleuse sample 8274: Axial deformation versus logarithm of time (detail)
3.5a	Marl grumeleuse sample 8293: Axial deformation versus square root of time
3.5b	Marl grumeleuse sample 8293: Axial deformation versus logarithm of time
3.5c	Marl grumeleuse sample 8293: Axial deformation versus logarithm of time (detail)
3.6	Reduction in deformation modulus as a function of deviator stress and creep rate
4.1	Results from triaxial swelling tests
4.2	Results from triaxial swelling tests
5.1	Composition and inferred swelling potential of molasse marls in comparison with other marl formations
5.2	Correlations of swelling mineral content with swelling behaviour
6.1	1-D Swelling (normal to bedding). Data from additional investigations
6.2	1-D Swelling data (normal to bedding) Data from original investigations
6.3	1-D Swelling data (normal to bedding) - Summary curves
6.4	1-D Swelling data (normal to bedding) - All Data and Design Curves

1 INTRODUCTION

This report presents the assessment and interpretation of additional geotechnical laboratory testing of core samples of marl and marl grumeleuse from the Point 5 site. These tests provided additional data on the effective strength parameters and in particular the creep and swelling properties of the Molasse. These data are required to confirm the parameters used to represent these material properties during the Phases One and Two of the design process.

1.1 Scope of work

The Civil Engineering Consultancy Services for Package 02 are provided by GIBB-SGI-Geoconsult joint venture, in five phases of work. The work presented in this report provides supplemental data to that presented in the GIBB Geotechnical Interpretative Report (GIR) included in the Phase One preliminary design.

The work reported herein consists of specialised laboratory testing of samples of Molasse obtained from boreholes SLHC81 and 82 from the Point 5 site. These tests consisted of;

- 5 No. triaxial creep tests (performed at ISMES)
- 4 No. triaxial swelling tests (performed at Imperial College)
- 4 No. triaxial strength tests (performed at the Norwegian Geotechnical Institute)
- 12 No. Sets of one-dimensional swelling tests (performed at the Ecole Polytechnique Federale du Lausanne)

2 EFFECTIVE STRENGTH TESTS

2.1 Stress path testing

A total of nine triaxial tests were performed on samples of marl grumeleuse at the Norwegian Geotechnical Institute. The tests were consolidated undrained triaxial tests with pore pressure measurement. The tests were performed on 38 mm diameter samples with a minimum length to diameter ratio of 2. Details of the sample preparation and test procedure and a complete presentation of the factual data can be found in Reference 1.

From the stress analysis data presented in Figure 2.1a it was possible to idealise the likely stress paths experienced at specific locations in the rock during the cavern construction. Three stress paths were chosen to represent the in situ stress paths experienced at the locations of the cavern crown, springline and floor. The idealised effective stress paths used in the triaxial tests are summarised in Table 1 below and illustrated in Figure 2.1b.

Table 1: Idealised triaxial stress paths

	Field Representation	Triaxial stress path
Stress path #1	Crown (extension)	Axial stress constant Radial stress increasing
Stress path #2	Springline (compression)	Axial stress constant Radial stress decreasing
Stress path #3	Floor (extension)	Axial stress decreasing Radial stress constant

2.2 Overview of results

The results of the triaxial strength tests in terms of peak effective stresses at failure are summarised in Table 2. These data are also plotted in s' - t space in Figure 2.2. Also indicated on this plot are three additional data points; two (IC1 and IC2) were deduced from the triaxial swelling tests reported later in section 4 and one (PC1) from a triaxial compression test performed as part of the creep testing programme reported in Section 3.

The IC points indicate the approximate effective stress conditions at failure for two marl grumeleuse specimens tested in the triaxial swelling programme at Imperial College (see Section 4). Point IC1 was the effective stress condition just prior to the load increment which resulted in the immediate failure of one specimen, and the points marked IC2 indicate the effective stress load increment during which failure occurred for the other specimen. Since the pore pressures were not measured it is not possible to deduce the exact effective stress conditions at failure. The additional data point PC1 was obtained from a conventional undrained triaxial compression test on marl as part of the creep testing programme carried out at ISMES (see Section 3).

Table 2: Summary of triaxial strength tests

Test No.	Sample ID	Lithology**	Vertical depth (m)	Moisture content (%)	Unit weight (kN/m ³)	Consof. stress (MPa)*	Deviator stress at failure (MPa)*	Mean stress at failure (MPa)*	Applied stress path
1	8281	M/MG	109.18	7.27	24.39	4.0	-7.88	5.17	Floor
2	8281	M/MG	109.43	6.43	24.69	4.0	-11.34	7.00	Floor
3	8218	MG	66.90	9.61	23.64	3.0	-4.20	3.60	Crown
4	8218	MG	66.67	9.47	23.56	1.42	-2.40	1.75	Crown
5	8214	M	67.27	5.66	24.70	3.0	13.50	8.50	Springline
6	8214	M	67.40	5.53	24.79	1.5	12.50	8.40	Springline
7	8218	MG	66.74	9.34	23.73	0.7	-1.30	0.90	Crown
8	8214	M	67.20	5.17	24.14	0.75	5.80	3.75	Springline
9	8201	MG	55.86	8.90	23.59	0.99	2.40	1.70	Springline

*All stresses are effective stresses

** Marl (M), Marl Grumeleuse (MG), transitional lithology (M/MG)

There is some uncertainty concerning the exact lithology of some of the specimens tested, as it is difficult to determine detailed characteristics without using destructive logging techniques. Samples for tests 1 and 2 were logged as marl grumeleuse, although the grumeleuse texture was not as well developed as elsewhere. This is demonstrated by the low moisture contents (more typical of marls) and by the higher strengths measured for these specimens. Tests 3,4,7 and 9 were all performed on marl grumeleuse, whilst tests 5,6 and 8 were all conducted on samples of marl.

Figure 2.2 indicates that the peak strength observed for test 9 is the only marl grumeleuse test result that lies in compression space. This failure point lies above the assumed effective stress design envelope which is consistent with the fact that the design envelope is based on lower bound peak strengths.

In extension space, the results from tests 3, 4 and 7, plus the additional data from the triaxial swelling tests, can be used to derive a peak effective strength envelope for marl grumeleuse. This peak strength envelope (fitted by linear regression) is indicated by the solid line in Figure 2.2 and gives the following effective strength parameters

$$\phi_p' = 31.4^\circ \quad c' = 0.22 \text{ MPa.}$$

From the plots of deviator stress versus axial strain, shown in Figures 2.3a to 2.3i, values of the undrained modulus of deformation (E_{DU}) can be calculated from the relationship

$$E_{DU} = \frac{(\sigma_1 - \sigma_3)}{\epsilon_a} \quad (1)$$

where, $(\sigma_1 - \sigma_3)$ = deviator stress
 ϵ_a = axial strain.

The secant values of E_{DU} obtained from the triaxial tests are presented below in Table 3. As is often observed in geotechnical materials, the response of the material indicates an decrease in stiffness with increasing strain as indicated by the steeper initial portion of the curves, (see

Figure 2.3 a to i). The values of deformation moduli presented in Table 3 were obtained for axial strain levels greater than 0.05 %.

The high deformation moduli measured in tests 1 and 2 confirm that the grumeleuse texture is poorly developed and that these specimens are likely to be more marly in character, which would also be consistent with the high strengths measured for these samples.

It should be noted that the deformation modulus measured in the triaxial specimens reflect the stiffness of the intact rock, and not the large scale in situ stiffness which is likely to be reduced due to the presence of natural fractures in the rock mass.

Table 3: Derived values of deformation modulus from triaxial strength tests

Test No.	Sample ID	Lithology	Deformation modulus (MPa)
1	8281	M/MG	15000
2	8281	M/MG	7800
3	8218	MG	3000
4	8218	MG	2300
5	8214	M	7300
6	8214	M	6000
7	8218	MG	1500
8	8214	M	3500
9	8201	MG	1800

2.3 Effective Strength Tests - Conclusions

The strength envelope derived from the laboratory tests is a reflection of the peak strength of the intact rock. Consequently the failure envelope derived from these test lies (as expected) above the design envelope presented in Table 9.9 of the GIR which is based on residual strength parameters. The actual peak strengths mobilised in the rock mass are likely to be less than those obtained from the laboratory tests due to the jointed and fractured nature of the in situ rock mass. Furthermore, the in situ strength envelope is likely to be curved exhibiting greater peak strengths at low stress levels than a linear envelope.

The undrained modulus of deformation measured in the tests confirm that lower stiffnesses are associated with the marl grumeleuse material. Both the marl and marl grumeleuse indicate that the stiffness decreases with increasing strain.

Representative in situ stress paths from FE analysis (GEODES)

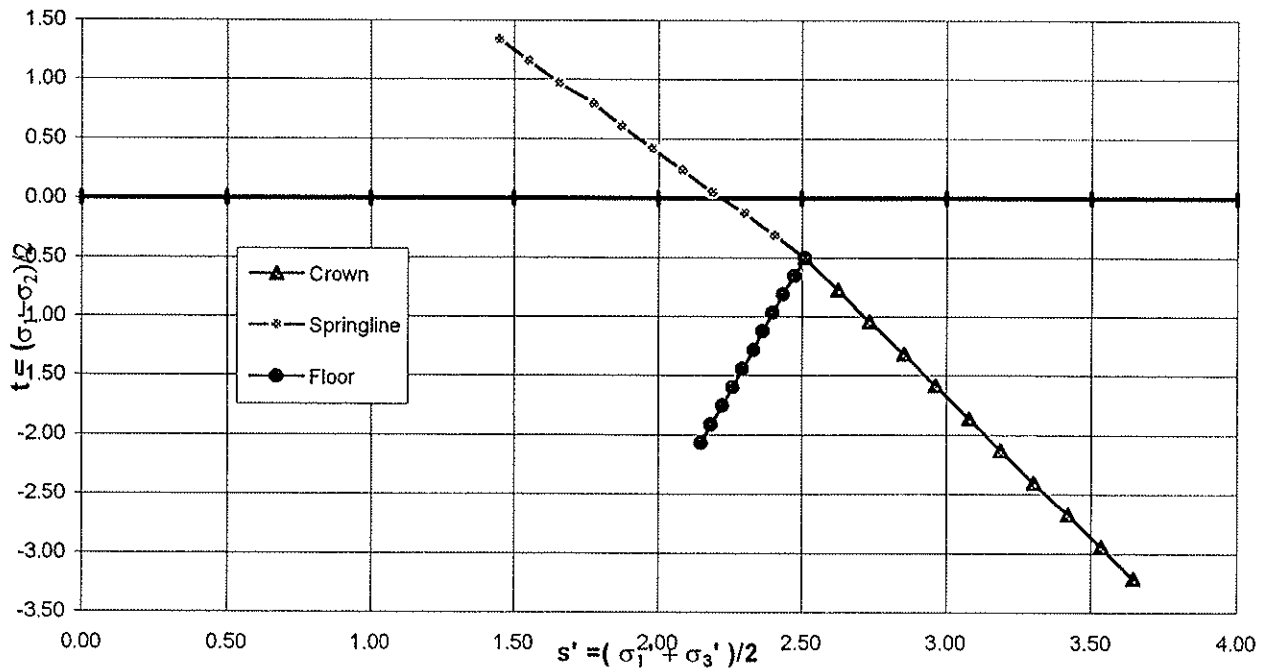


Figure 2.1 a

Conventional triaxial compression and extension stress paths

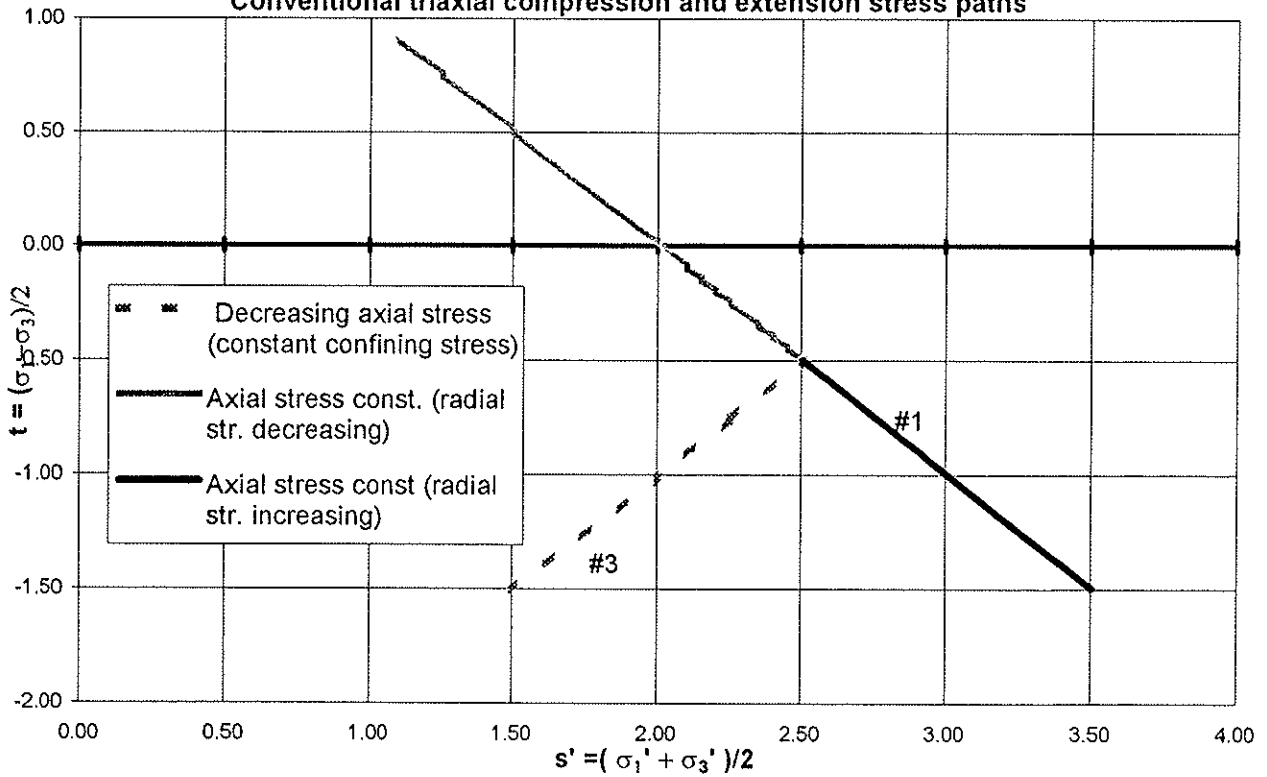


figure 2.1 b

GIBB



CERN - LHC PROJECT - POINT 5

J96107

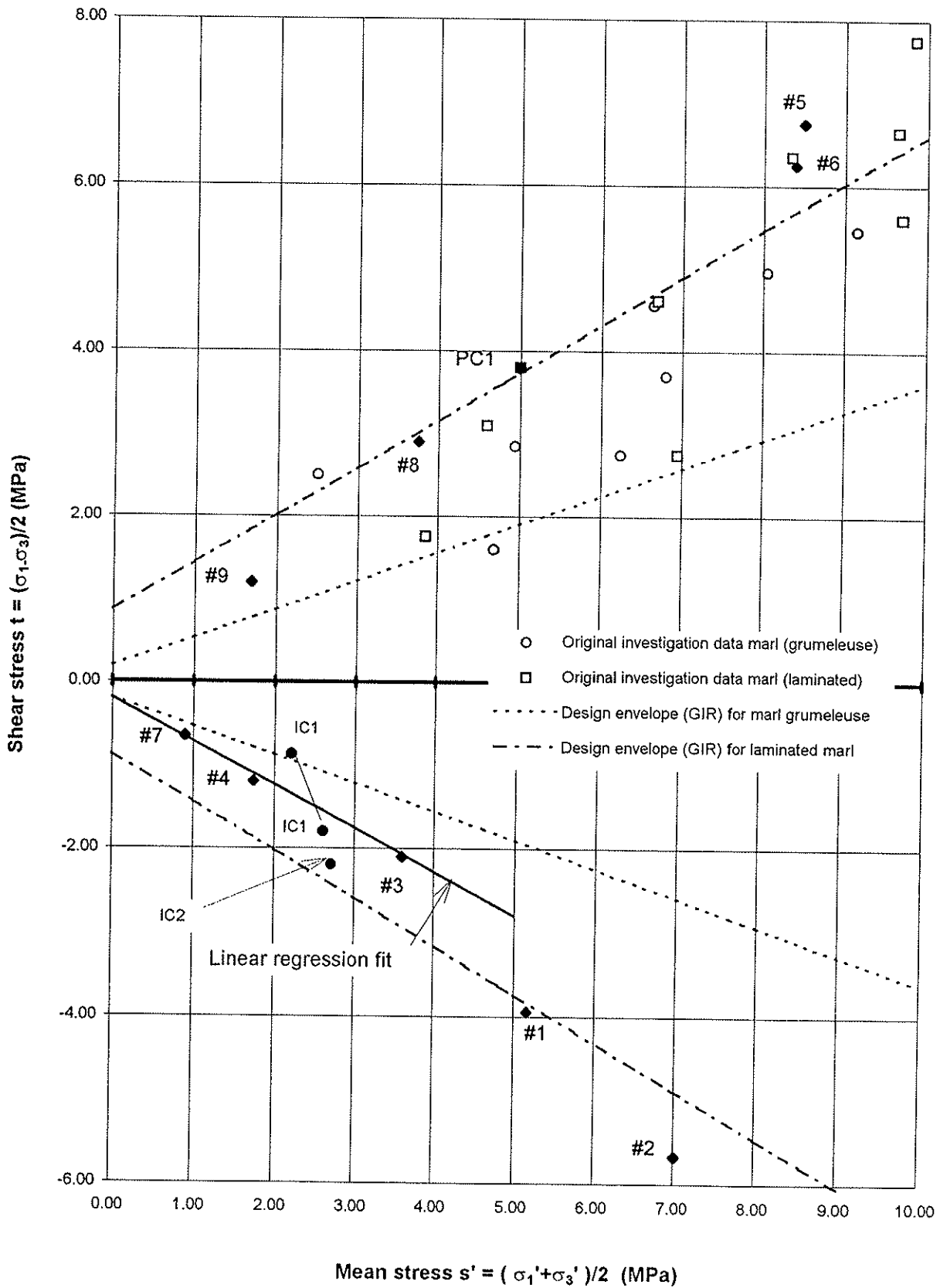


SGE INGENIERIE

a) CALCULATED IN SITU STRESS PATHS
AND b) IDEALISED TRIAXIAL
REPRESENTATIONS

Date
August
1997

Figure
2.1



GIBB



SGI INGENIERIE

CERN - LHC PROJECT - POINT 5

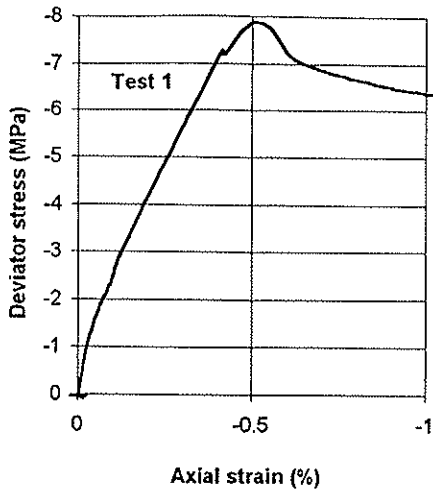
RESULTS FROM TRIAXIAL STRENGTH TESTS

J96107

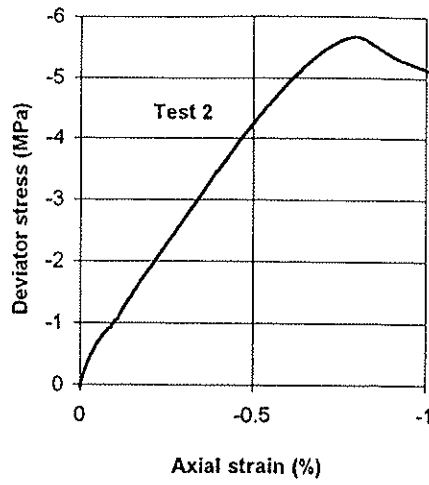
Date
August
1997

Figure

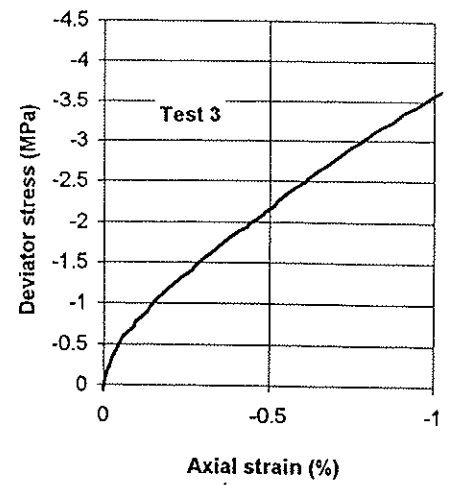
2.2



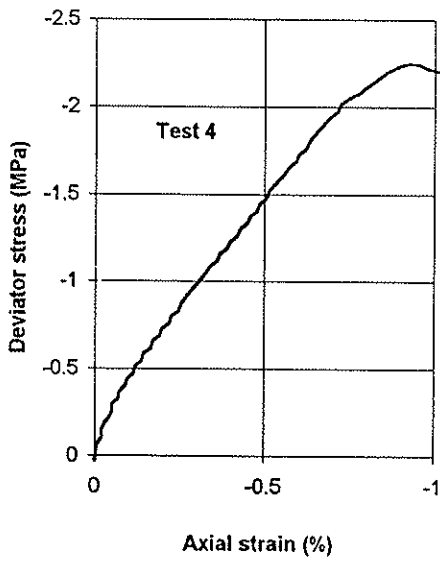
a



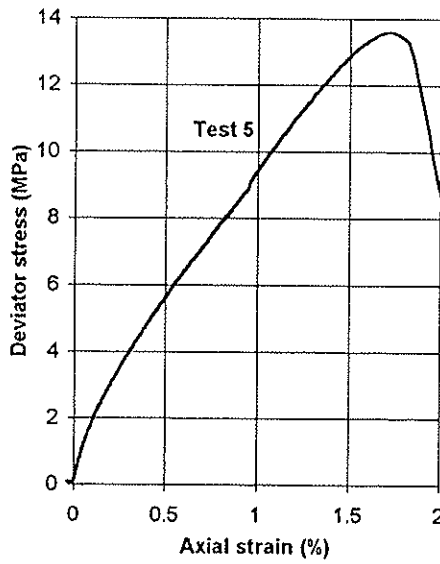
b



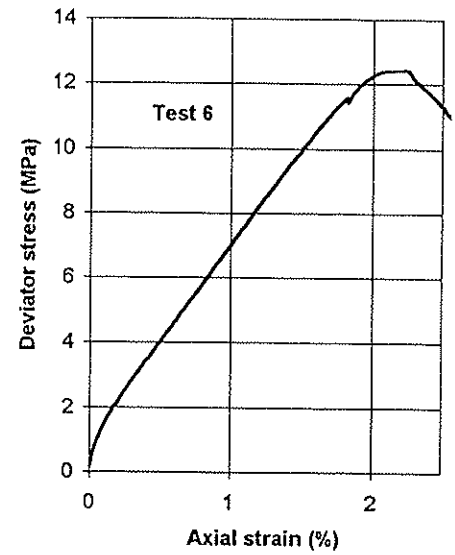
c



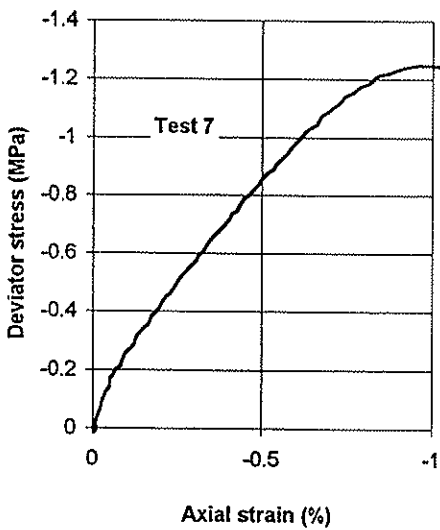
d



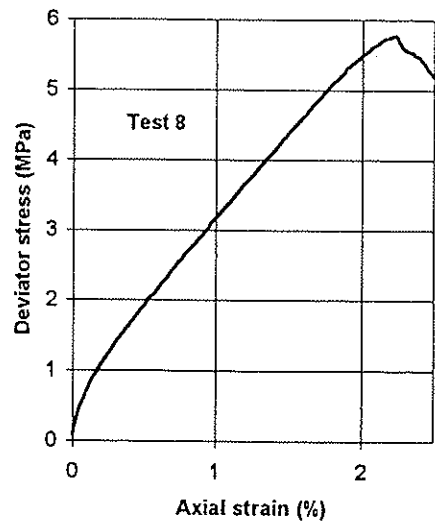
e



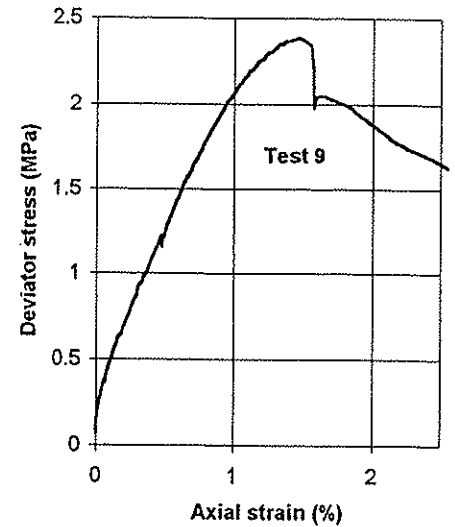
f



g



h



i

GIBB



CERN - LHC PROJECT - POINT 5

J96107

DEVIATOR STRESS VERSUS AXIAL STRAIN
PLOTS FROM TRIAXIAL STRENGTH TESTS

Date
August
1997

Figure
2.3

SEI INGENIERIE

3 TRIAXIAL CREEP TESTS

3.1 Introduction

Five triaxial creep tests were performed at ISMES, Bergamo. The test specimens were 50 mm in diameter with a minimum length to diameter ratio of 2. Each test was performed as a conventional drained triaxial compression test with a 0.5 MPa back pressure but each axial load increment was maintained for a period of several weeks with continuous monitoring of the specimen axial and radial strains. Details of the test method and a complete presentation of the factual data can be found in Reference 2.

3.2 Applied loading

The incremental loads applied to the samples were approximately 25, 50 or 75% of the estimated deviatoric stresses at failure. Due to time constraints on the testing programme, it was not possible to apply all three load increments to every sample, but sufficient data has been obtained to evaluate the creep response of the materials tested over the full range of likely induced stresses. The test programme is summarised in Table 4 below.

Table 4: Loading history for creep tests

Sample (M) - Mari (MG) - Marl Grumeleuse	Confining pressure (MPa)*	Estimated ($\sigma_1 - \sigma_3$) _f at failure (MPa)*	Cycle 1 25 % of ($\sigma_1 - \sigma_3$) _f (MPa)*	Days under load	Cycle 2 50 % of ($\sigma_1 - \sigma_3$) _f (MPa)*	Days under load	Cycle 3 75 % of ($\sigma_1 - \sigma_3$) _f (MPa)*	Days under load
8139 (M)	0.7	3.39	0.847	15.5	1.695	74	2.542	-
8159 (M)	2.0	5.91	1.477	33	-	0	4.432	9**
8143 (MG)	0.7	1.05	0.262	26	0.525	16	0.787	38
8274 (MG)	2.0	2.28	0.570	61	1.140	-	1.710	-
8293 (MG)	3.0	3.35	0.837	10	1.675	73	2.512	-

*All stresses are effective stresses.

** Test finished prematurely due to hydraulic failure

After completion of the creep loading cycles, undrained tests to failure were to be performed. The results of these tests are presented in detail in Reference 2.

3.3 Overview of results

The data from the triaxial creep tests are best presented in plots of axial strain versus time. For each test, plots of axial strain versus square root of time, and axial strain versus \log_{10} of time are presented, see Figures 3.1 to 3.5.

To enable each load cycle for any one test to be plotted on the same graph, the time has been reset to zero at the start of each loading cycle. The axial strain measured in the tests is initially dominated by elastic deformation and by primary consolidation. After dissipation of pore pressures, continuing deformation is due to creep (otherwise known as secondary consolidation).

The approach adopted to modify the long term stiffness based on the triaxial creep tests was as follows;

- It was assumed that the time for completion of the primary consolidation stage for each load increment was 10 000 minutes (approximately 1 week).
- The slope of the plot of axial strain against logarithm of time was deduced for the secondary consolidation (creep) response stage of the tests. This slope is conventionally denoted as C_α such that

$$C_\alpha = \frac{\Delta \varepsilon_c}{\log_{10} \left(\frac{t_2}{t_1} \right)} \quad (2)$$

where $\Delta \varepsilon_c$ is the cumulative creep strain over the period t_1 to t_2 .

- The value of C_α can then be used to extrapolate the total creep strain that occurs over the 50 year design life of the structures at Point 5.
- Using this value of creep strain an indication in the reduction in initial deformation modulus prior to creep can be estimated from the ratio of deviator stress to total axial strain at 50 years.

For the analysis presented here, the initial modulus prior to creep deformation (E_{D1}) is taken as the deformation modulus at the assumed end of primary consolidation. This is calculated from the ratio of deviator stress to corresponding axial strain (ε_i) 10000 minutes after the application of load. The value of deformation modulus at 50 years is calculated from the ratio of deviator stress to total axial strain at 50 years. Thus the ratio between initial deformation modulus and the final modulus after 50 years of creep stain (E_c) is given by

$$\frac{E_c}{E_{D1}} = \frac{\varepsilon_i}{\varepsilon_i + \Delta \varepsilon_c} \quad (3)$$

It should be noted that implicit in this relationship is the assumption that the creep rate increases linearly with deviatoric load. If the creep rate is a non-linear function of the applied deviator stress then the revised deformation modulus would also be non-linear in deviatoric stress - axial strain space, see Figure 3.6.

From the data presented in Figures 3.1(a-c) to 3.5(a-c) values of C_α have been estimated (where possible) for each load increment and are presented below in Table 5.

Table 5 : Summary of results from creep tests

Sample (M) - Marl (MG) - Marl Grumeleuse	Cycle 1 25 % of $(\sigma_1 - \sigma_3)_i$ (MPa)*	Days under load	C_α $\times 10^{-4}$	Cycle 2 50 % of $(\sigma_1 - \sigma_3)_i$ (MPa)*	Days under load	C_α $\times 10^{-4}$	Cycle 3 75 % of $(\sigma_1 - \sigma_3)_i$ (MPa)*	Days under load	C_α $\times 10^{-4}$
8139 (M)	0.847	15.5	-	1.695	74	7.15	-	-	-
8159 (M)	1.477	33	7.50	-	-	-	4.432	9	-
8143 (MG)	0.262	26	7.53	0.525	16	-	0.787	38	8.87
8274 (MG)	0.570	61	6.0	-	-	-	-	-	-
8293 (MG)	0.837	10	-	1.675	73	2.81	2.512	-	-

Using these values of C_α the reduction in the initial deformation moduli after 6 months (which is relevant to the construction period) and for the 50 year design life of the structure have been estimated using the procedure described above, and are summarised in Table 6 below.

Using these values of C_α the reduction in the initial deformation moduli after 6 months (which is relevant to the construction period) and for the 50 year design life of the structure have been estimated using the procedure described above, and are summarised in Table 6 below.

Table 6: Deformation moduli and reduction factors for creep

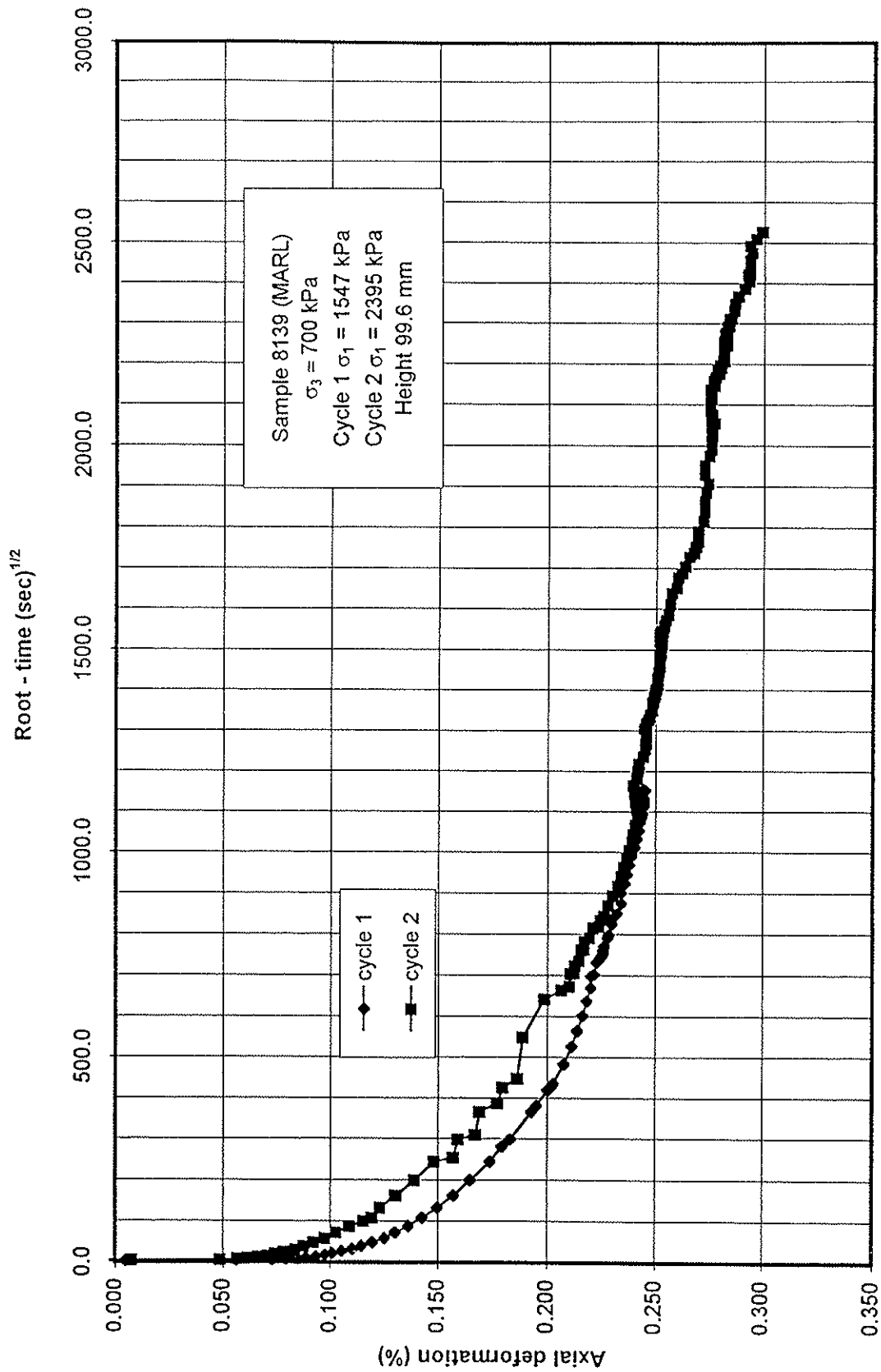
Sample (M) - Mari (MG) - Mari Grumelouse	Deviator stress (MPa)	Initial deformation modulus (MPa)	6 mths deformation modulus (MPa)	50 year deformation modulus (MPa)	Reduction in initial deformation modulus after 6 mths creep (%)	Reduction in initial deformation modulus after 50 yrs creep (%)
8139 (M)	0.847	385	263	182	32	53
8159 (M)	1.477	394	307	234	22	40
8143 (MG)	0.262	250	123	72	50	71
	0.787	624	312	183	50	70
8274 (MG)	0.570	356	232	156	35	56
8293 (MG)	0.837	945	672	462	29	51

3.4 Triaxial Creep Tests - Conclusions

From the limited data available a reduction in long term stiffness of between 40 and 70 % is indicated. These data are consistent with the design assumption of a 70 % reduction in the value of the deformation modulus due to long term creep (i.e. the long term modulus is 30% of the initial value, CREEP 2 case in Reference 7).

Using the creep parameters presented in Table 5 the short term creep effects can also be assessed. Table 6 indicates that a reduction of 20 - 50 % of the initial deformation modulus may occur at 6 months into the construction phase, (i.e. 50 to 80% of the initial modulus). This is consistent with the 50 % reduction in deformation modulus assumed to model short term creep effects (CREEP 1 case in Reference 7).

The secondary liner will be required to take the loading associated with the 20% reduction in the deformation modulus from the short (6 month case) to the long term condition.



GIBB



SGI INGENIERIE



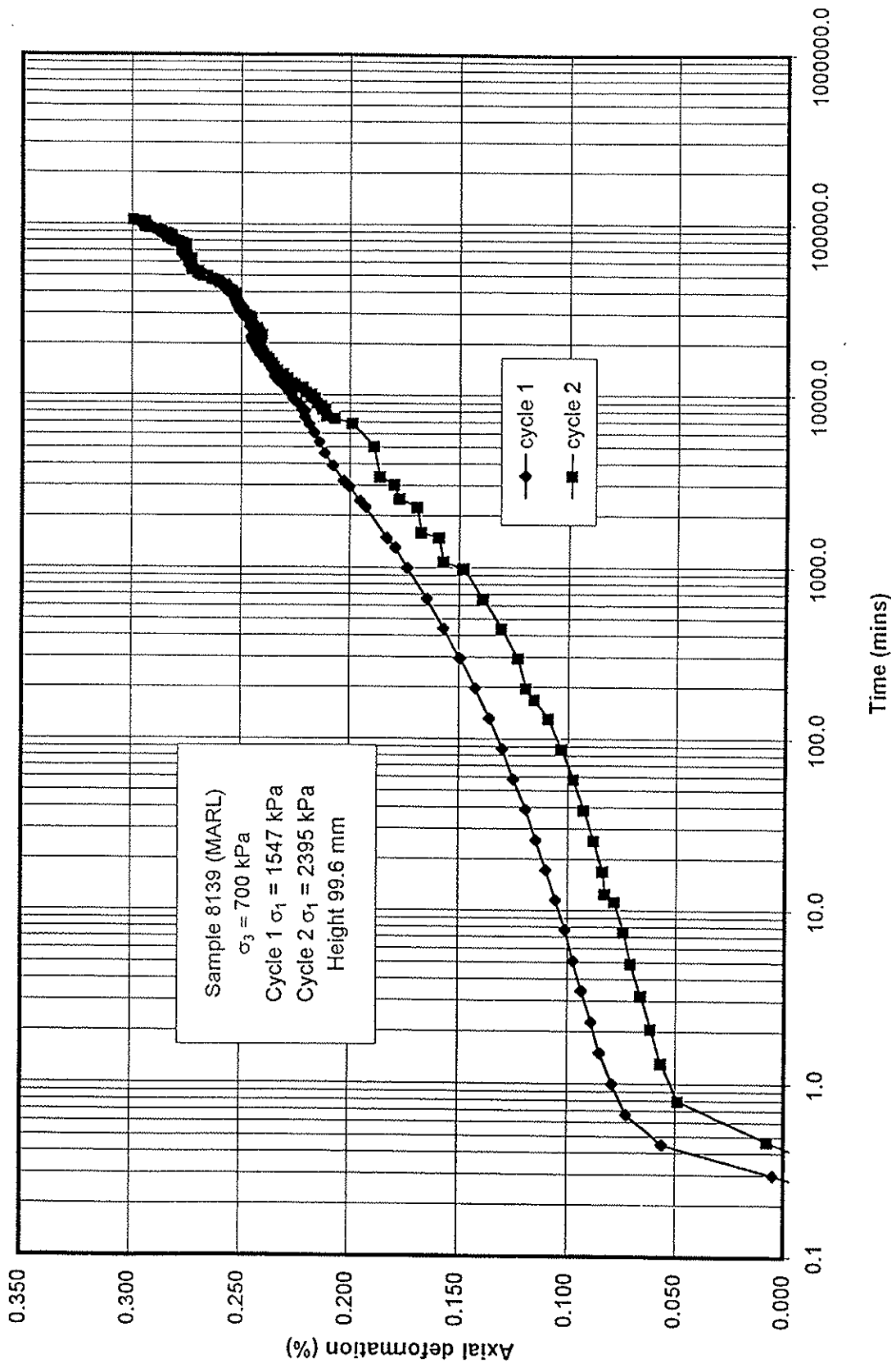
CERN - LHC PROJECT - POINT 5

MARL SAMPLE 8139
 AXIAL DEFORMATION VERSUS SQUARE
 ROOT OF TIME

J96107

Date
 August
 1997

Figure
3.1a



GIBB



SGI INGENIERIE



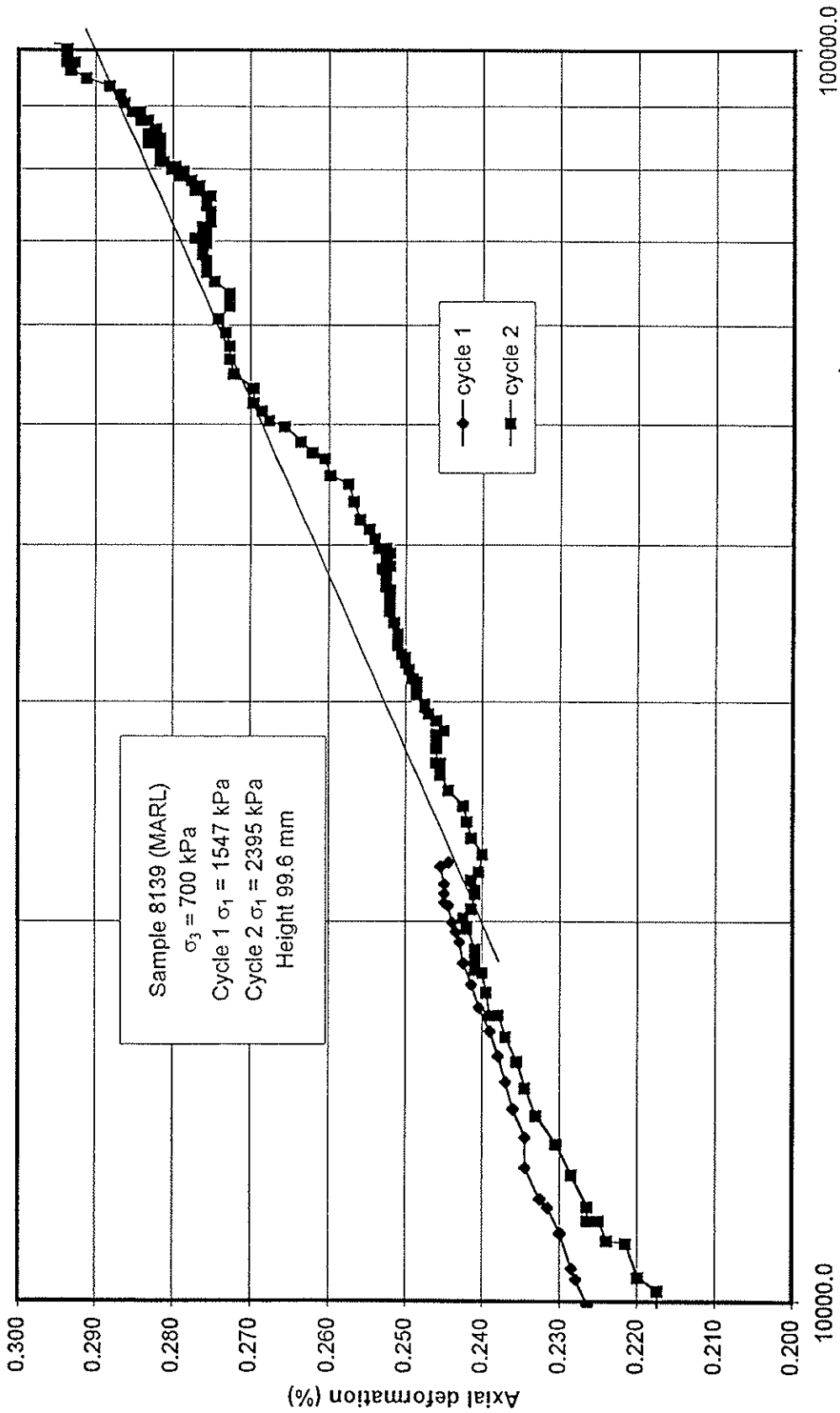
CERN - LHC PROJECT - POINT 5

MARL SAMPLE 8139
 AXIAL DEFORMATION VERSUS
 LOGARITHM OF TIME

J96107

Date
 August
 1997

Figure
3.1b



GIBB



SGI INGENIERIE



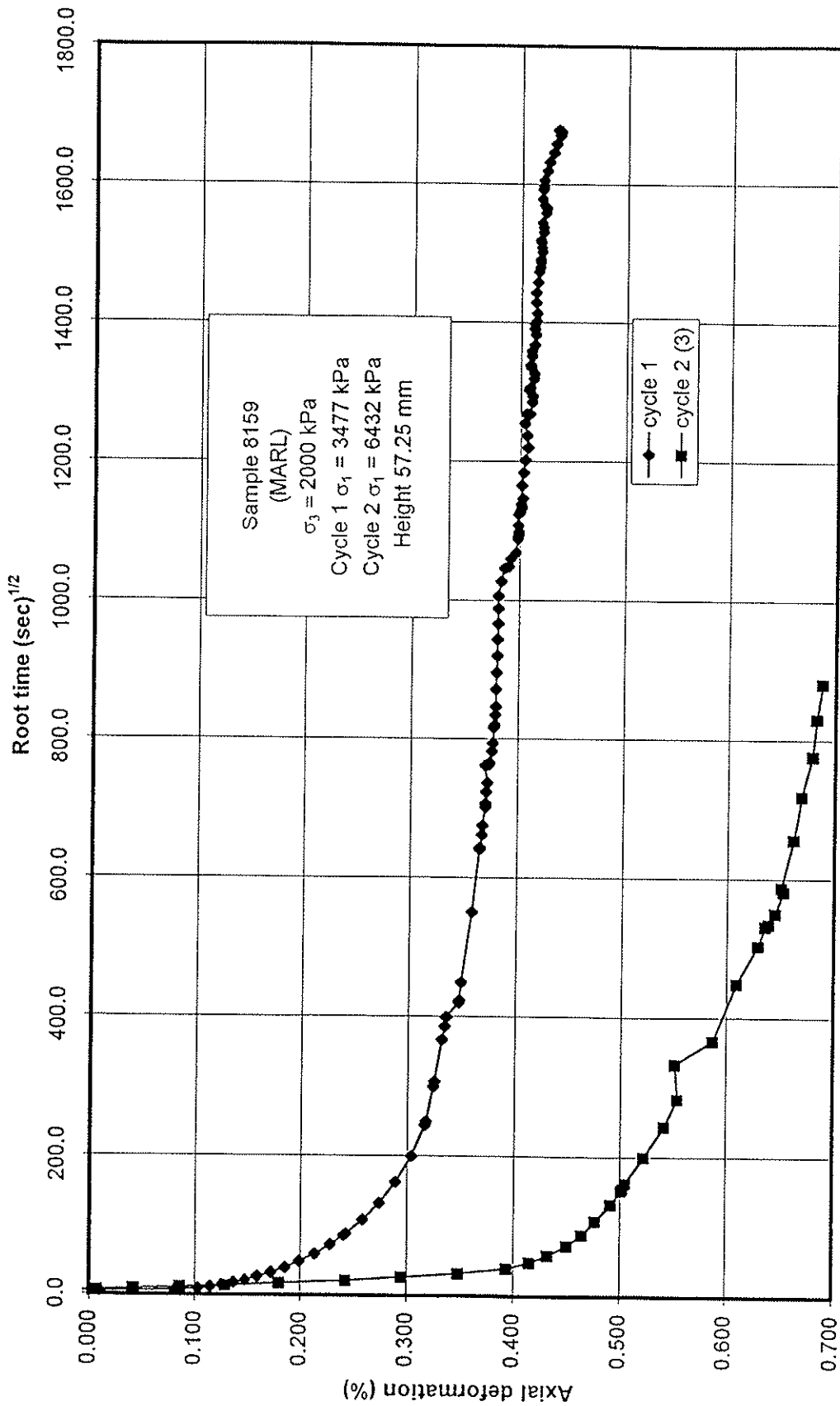
CERN - LHC PROJECT - POINT 5

MARL SAMPLE 8139
 AXIAL DEFORMATION VERSUS
 LOGARITHM OF TIME (DETAIL)

J96107

Date
 August
 1997

Figure
3.1c



GIBB



SEI INGENIERIE



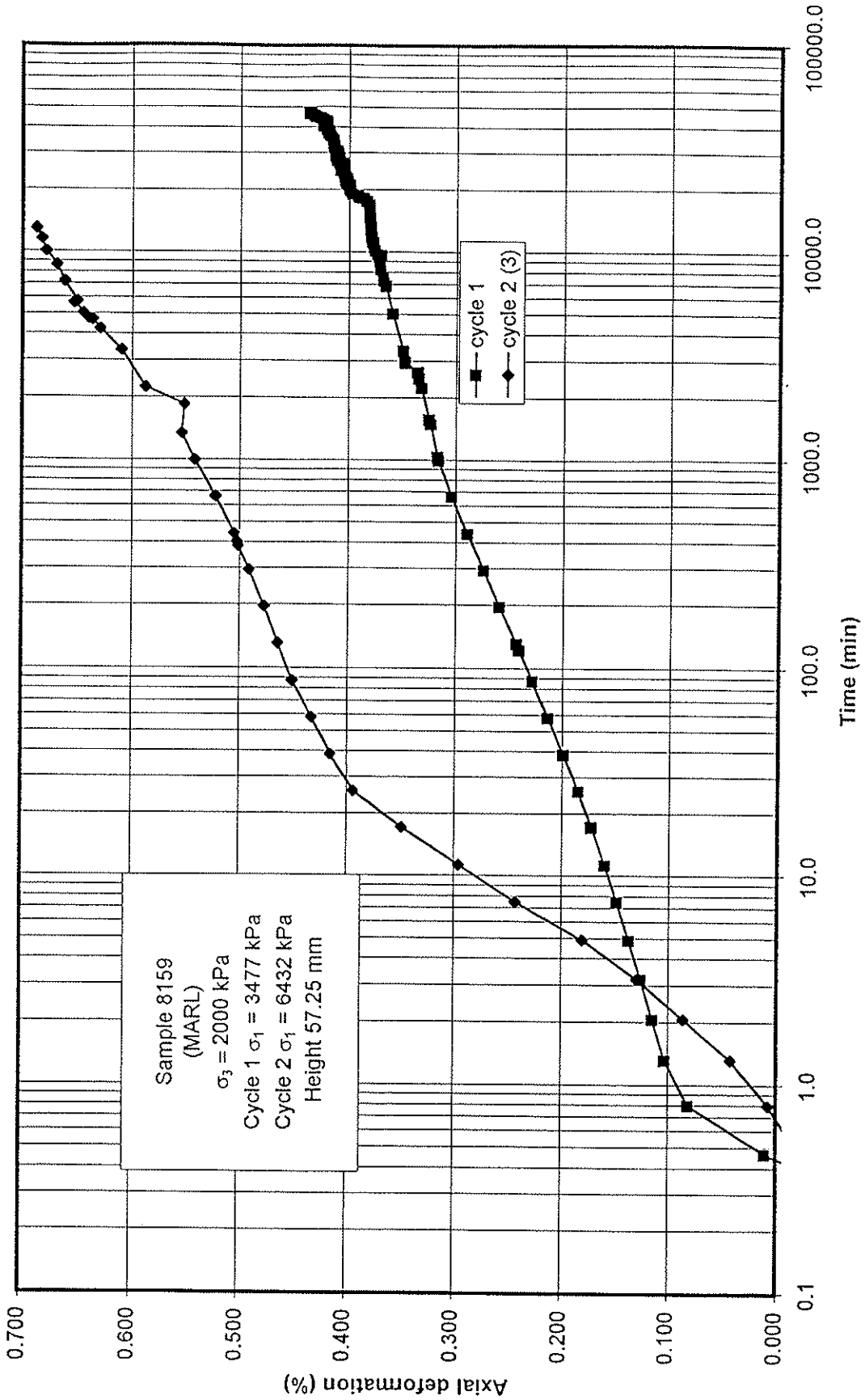
CERN - LHC PROJECT - POINT 5

MARL SAMPLE 8159
AXIAL DEFORMATION VERSUS SQUARE
ROOT OF TIME

J96107

Date
August
1997

Figure
3.2a



GIBB



SGI INGENIERIE

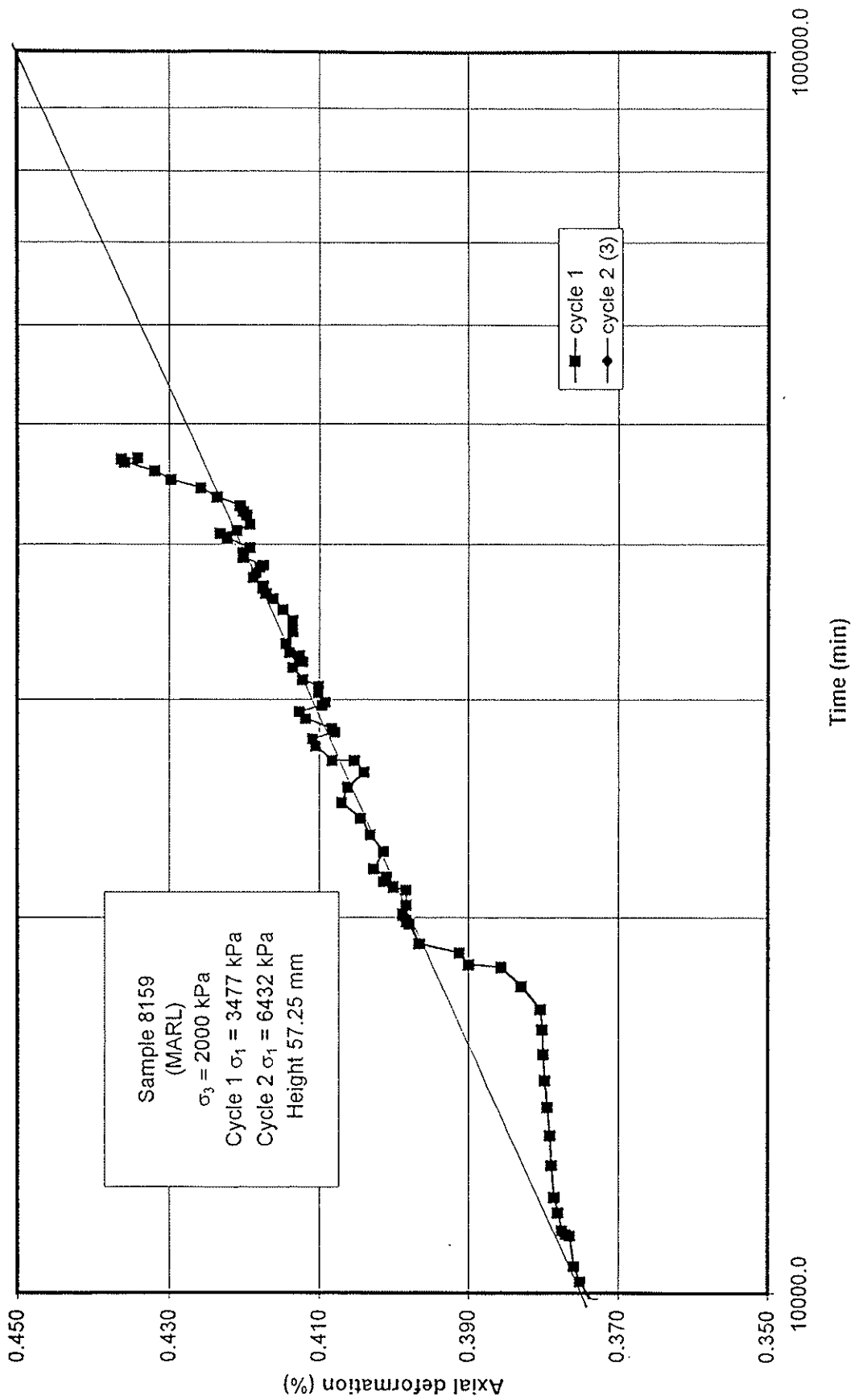
CERN - LHC PROJECT - POINT 5

MARL SAMPLE 8159
 AXIAL DEFORMATION VERSUS
 LOGARITHM OF TIME (DETAIL)

J96107

Date
 August
 1997

Figure
 3.2b



GIBB



SGI INGENIERIE



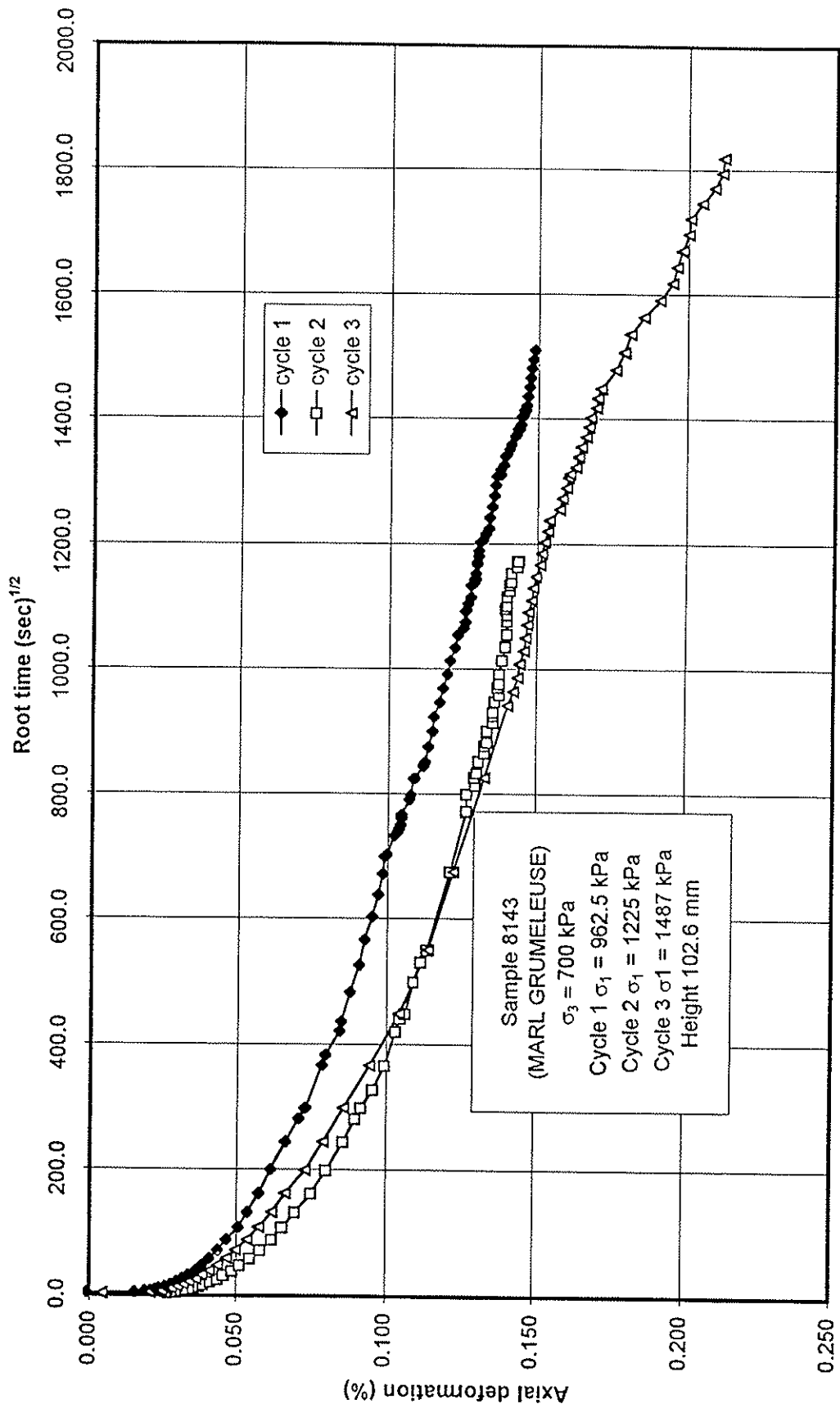
CERN - LHC PROJECT - POINT 5

MARL SAMPLE 8159
AXIAL DEFORMATION VERSUS
LOGARITHM OF TIME (DETAIL)

J96107

Date
August
1997

Figure
3.2c



GIBB



SGI INGENIERIE

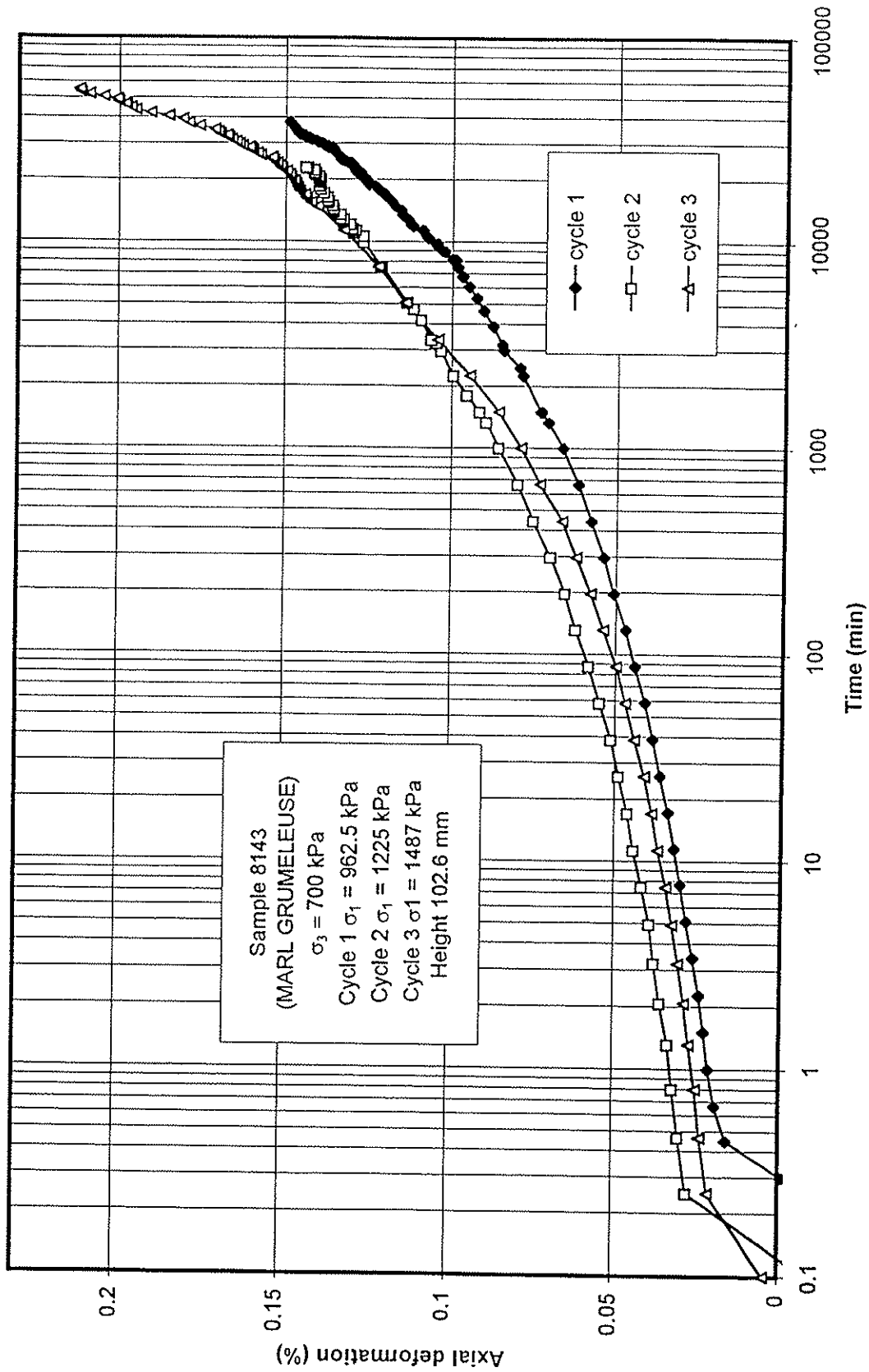
CERN - LHC PROJECT - POINT 5

J96107

MARL GRUMELEUSE SAMPLE 8143
 AXIAL DEFORMATION VERSUS SQUARE
 ROOT OF TIME

Date
 August
 1997

Figure
 3.3a



GIBB



SGI INGENIERIE

CERN - LHC PROJECT - POINT 5

MARL GRUMELEUSE SAMPLE 8143
 AXIAL DEFORMATION VERSUS
 LOGARITHM OF TIME (DETAIL)

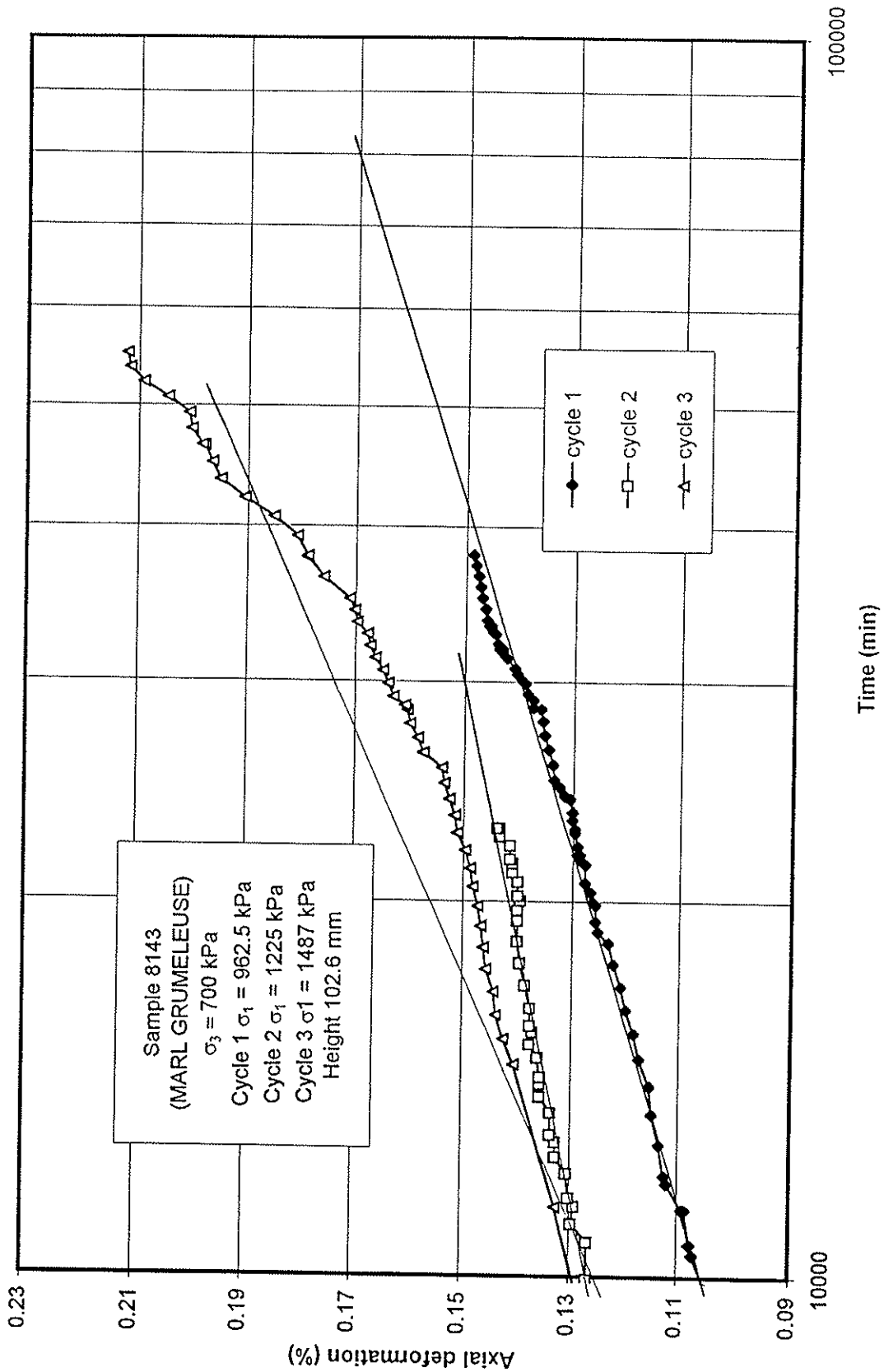
J96107

Date

August
 1997

Figure

3.3b



GIBB



INGENIERIE

CERN - LHC PROJECT - POINT 5

J96107

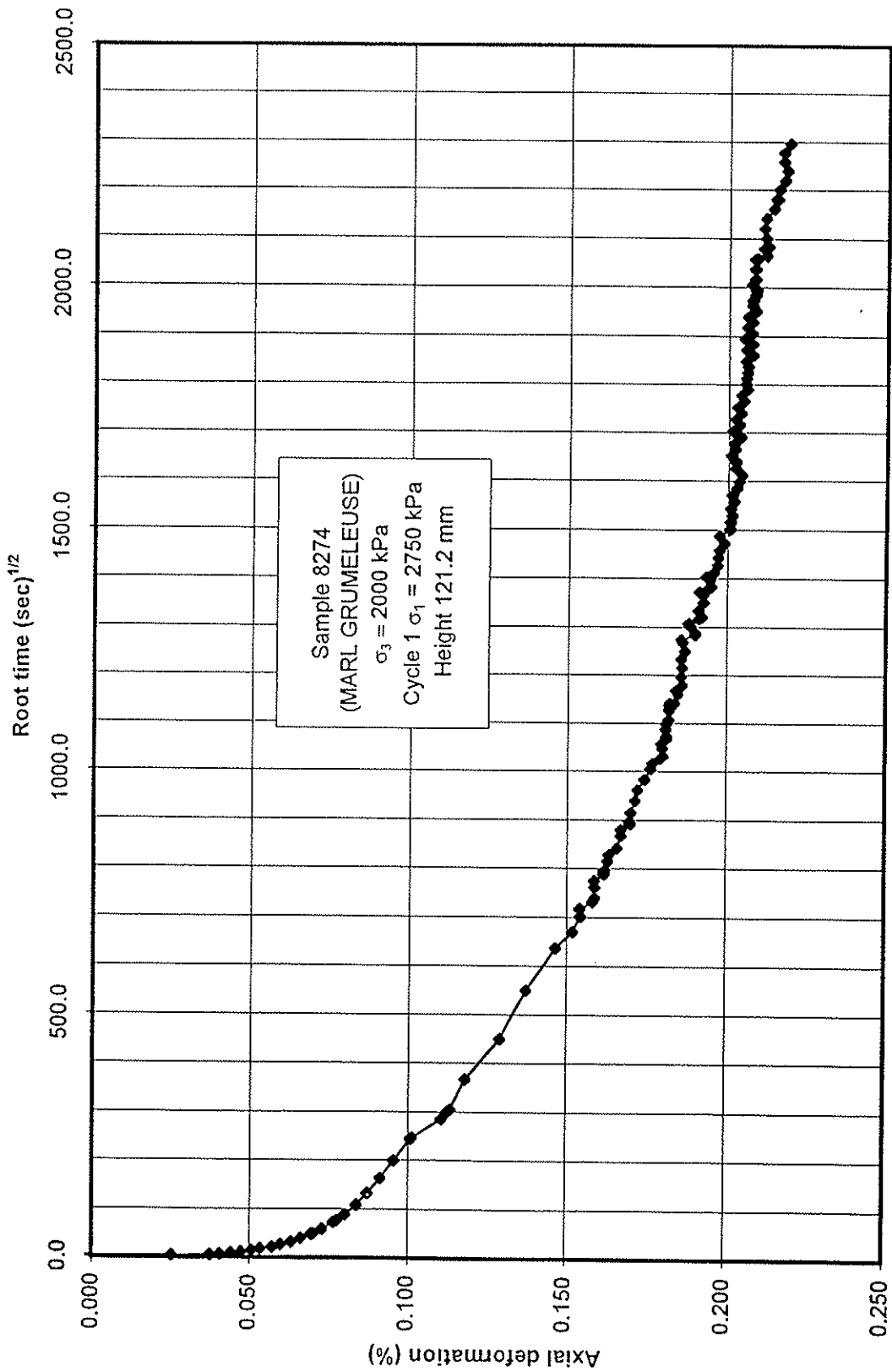
MARL GRUMELEUSE SAMPLE 8143
 AXIAL DEFORMATION VERSUS
 LOGARITHM OF TIME (DETAIL)

Date

August
 1997

Figure

3.3c



GIBB



SGI INGENIERIE



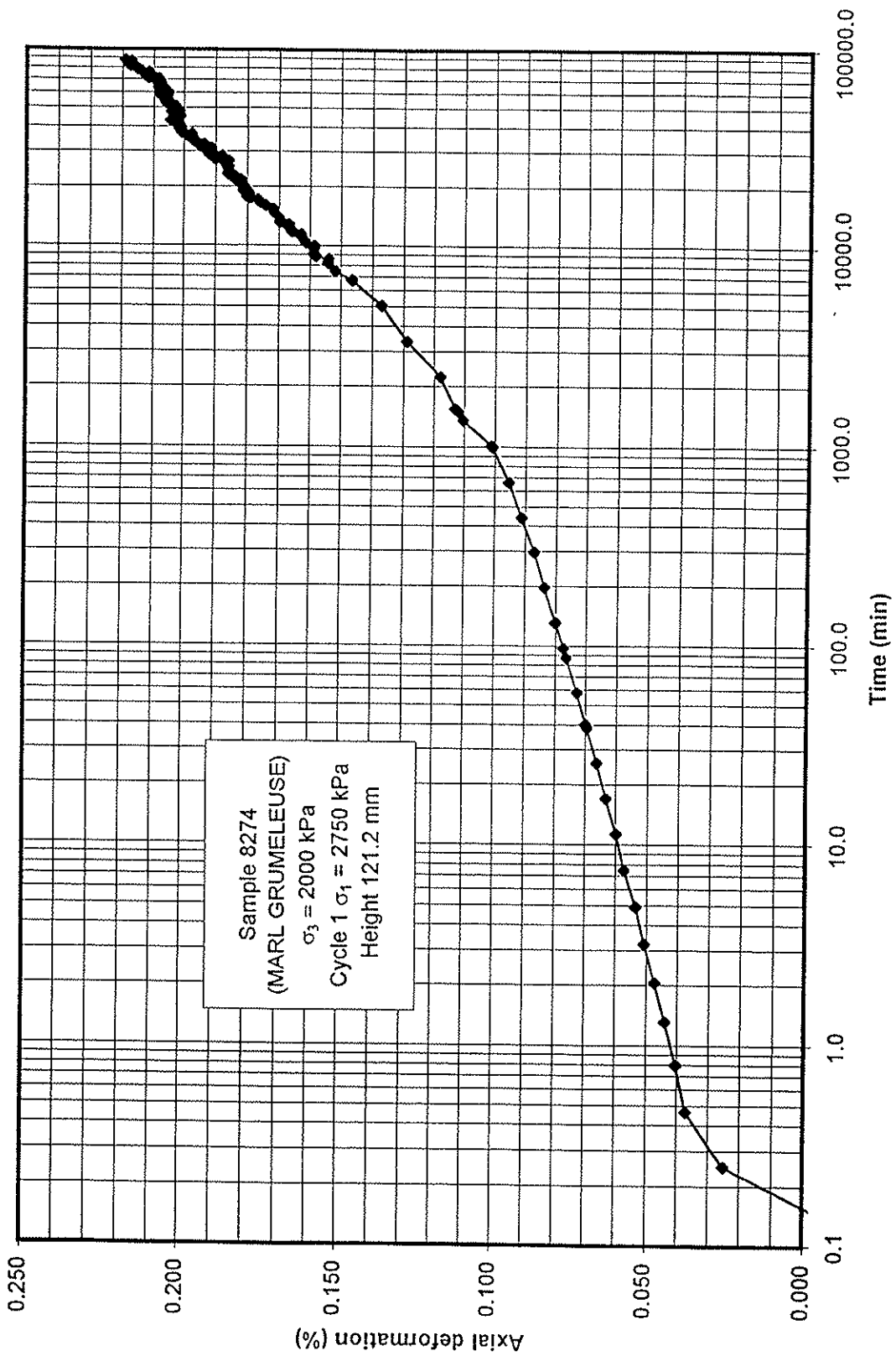
CERN - LHC PROJECT - POINT 5

MARL GRUMELEUSE SAMPLE 8274
AXIAL DEFORMATION VERSUS SQUARE
ROOT OF TIME

J96107

Date
August
1997

Figure
3.4a



GIBB



SGI INGENIERIE

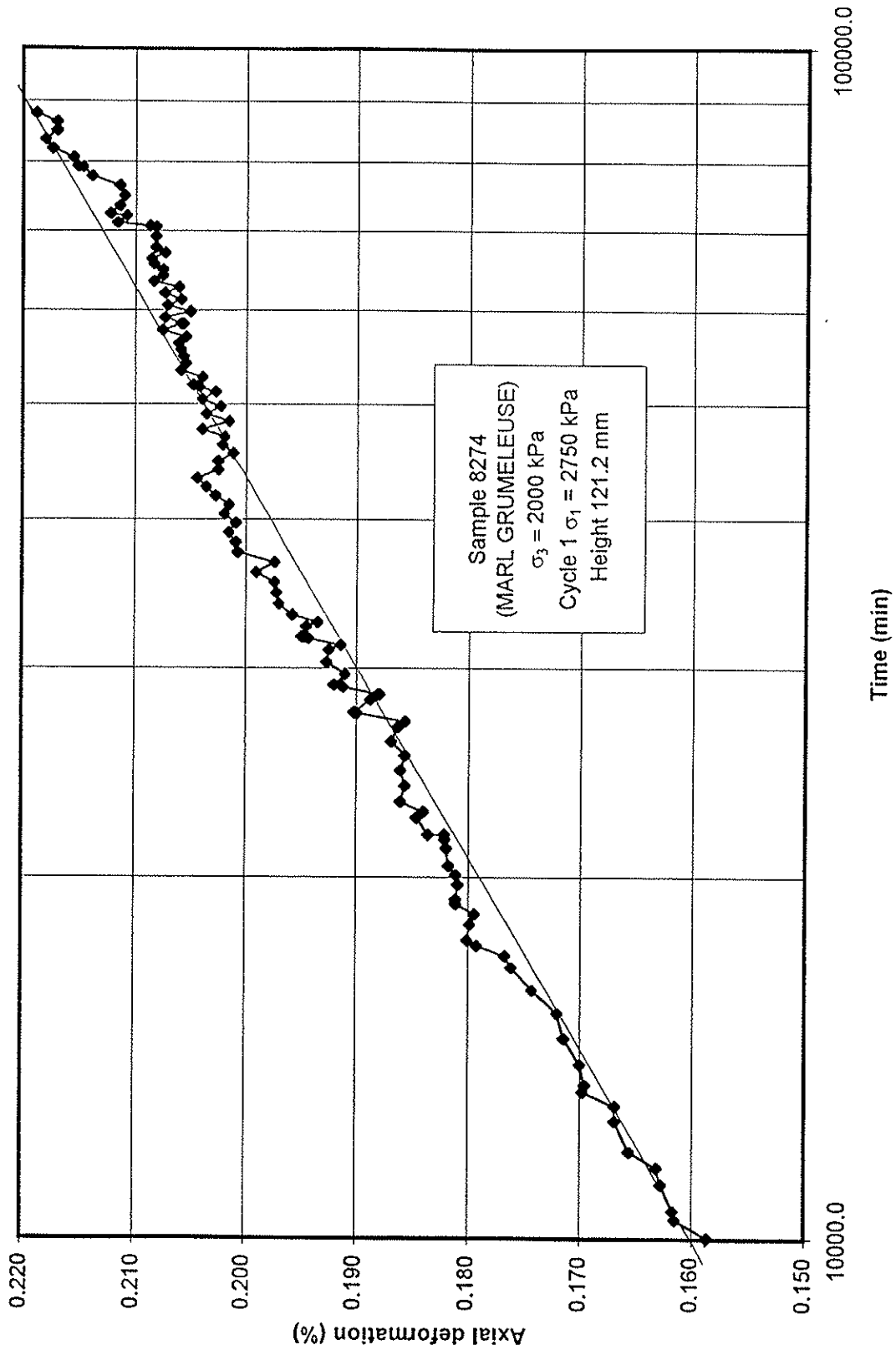
CERN - LHC PROJECT - POINT 5

MARL GRUMELEUSE SAMPLE 8274
AXIAL DEFORMATION VERSUS
LOGARITHM OF TIME (DETAIL)

J96107

Date
August
1997

Figure
3.4b



GIBB



SEI INGENIERIE



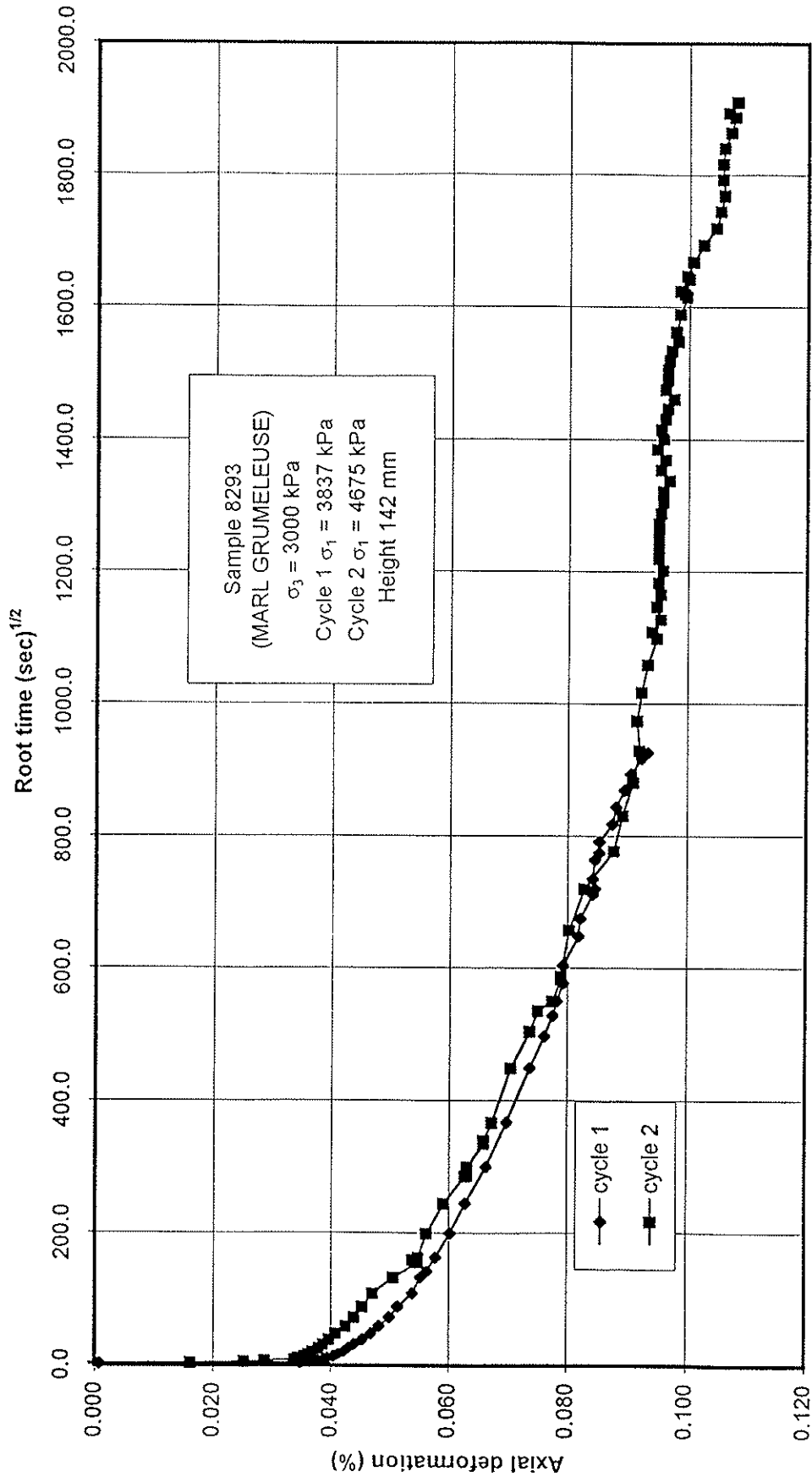
CERN - LHC PROJECT - POINT 5

MARL GRUMELEUSE SAMPLE 8274
AXIAL DEFORMATION VERSUS
LOGARITHM OF TIME (DETAIL)

J96107

Date
August
1997

Figure
3.4c



GIBB



SGI INGENIERIE



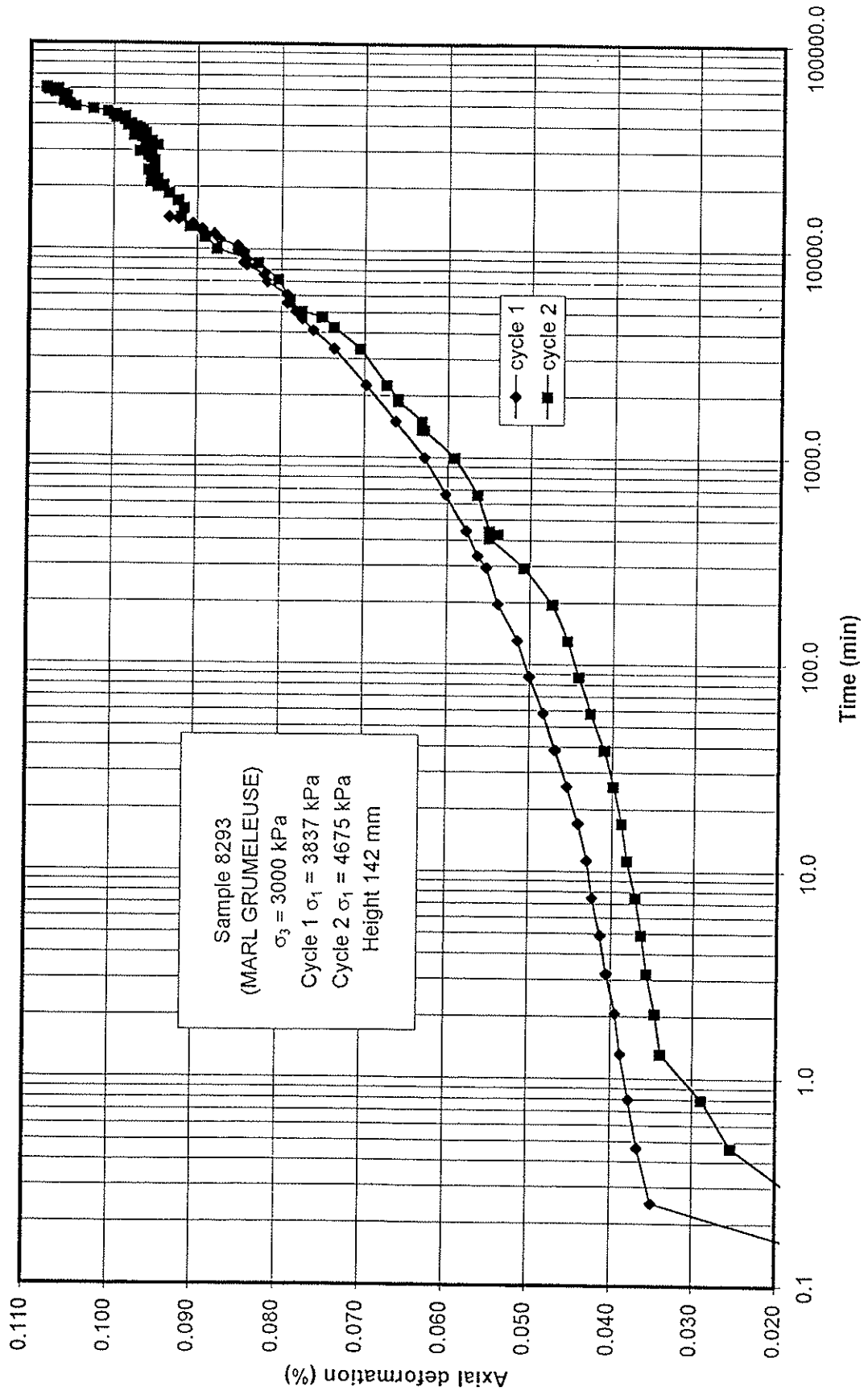
CERN - LHC PROJECT - POINT 5

MARL GRUMELEUSE SAMPLE 8293
AXIAL DEFORMATION VERSUS SQUARE
ROOT OF TIME

J96107

Date
August
1997

Figure
3.5a



GIBB



SGI INGENIERIE



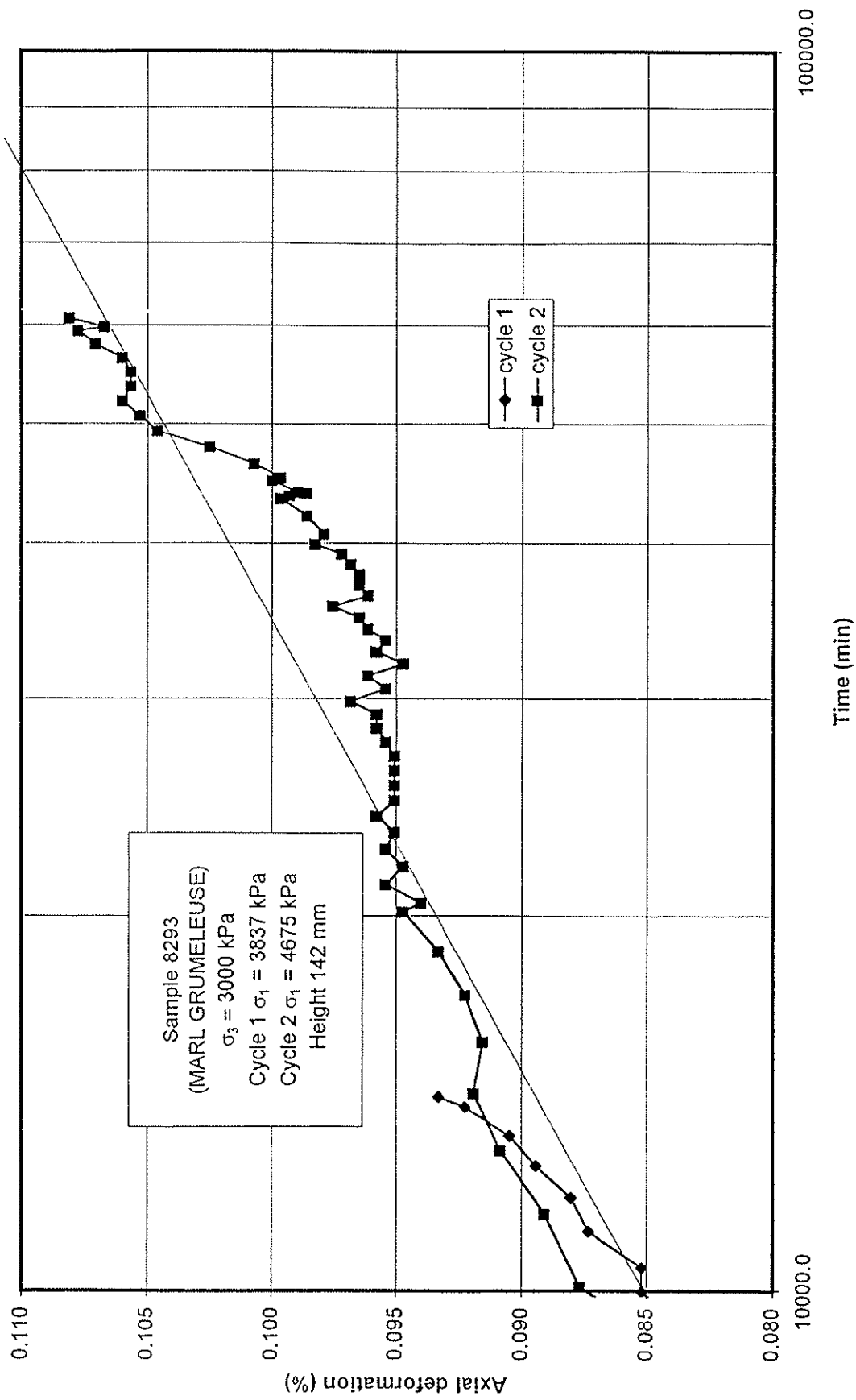
CERN - LHC PROJECT - POINT 5

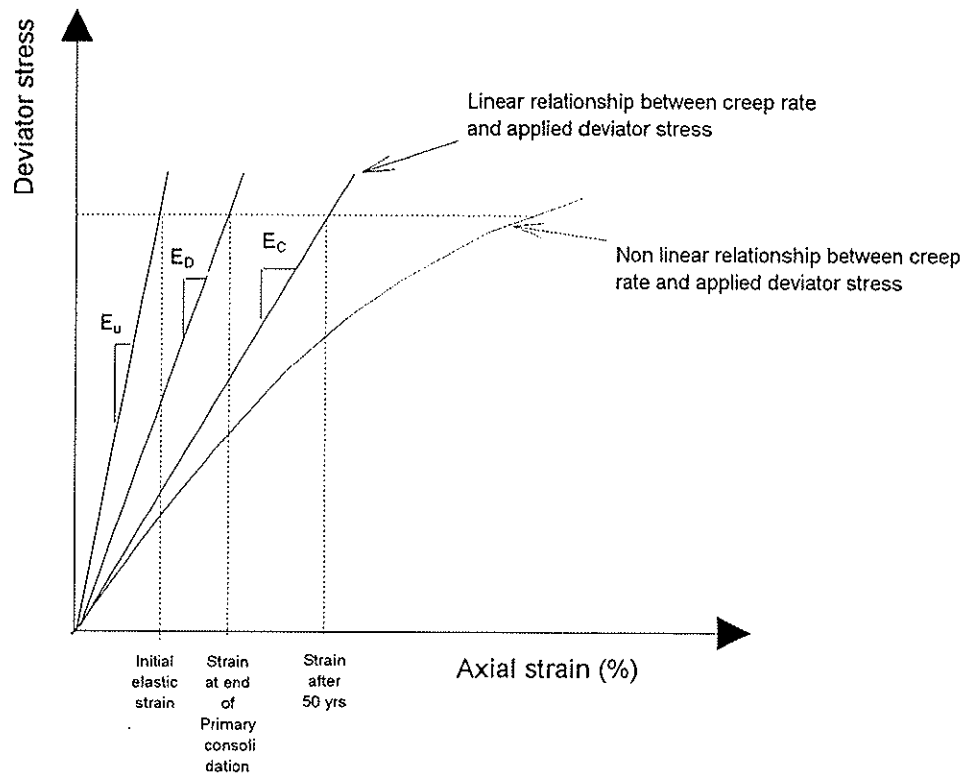
MARL GRUMELEUSE SAMPLE 8293
 AXIAL DEFORMATION VERSUS
 LOGARITHM OF TIME (DETAIL)

J96107

Date
 August
 1997

Figure
 3.5b





4 TRIAXIAL SWELLING TESTS

4.1 Introduction

Triaxial swelling tests were intended to provide data on the relationship between the applied stress level and swelling response of the marl grumeleuse material.

Two tests were completed by Imperial College Consultants Ltd. at the Royal School of Mines, Imperial College, London. An additional two tests were also performed but premature failure of the specimens occurred before completion of the tests. The tests were performed on 54 mm diameter specimens with height to diameter ratios of 1. Each test is effectively a drained triaxial test where all swelling (i.e. pore fluid movement) must cease prior the application of further load increments. The very low permeability of the marl grumeleuse material meant that each load increment took approximately one week to stabilise.

Details of the test method and a complete presentation of the factual data can be found in Reference 3.

4.2 Applied loading

It was intended that the triaxial stress paths would match as closely as possible the stress paths predicted from finite element calculations as shown in Figure 1a. These stress paths are assumed to represent the typical stress paths experienced by rock elements located a short distance (< 5 m) behind the excavated surface at the crown, springline and floor of the cavern. Due to time restraints on the testing schedule it was only possible to complete swelling tests following springline and crown stress paths, see Table 1 section 2.1.

4.3 Overview of results

The results of the triaxial swelling tests are summarised in Table 6. For each test the following plots are presented;

- Volumetric, axial and radial strain against mean effective stress (Figures 4.1a and 4.2a)
- Volumetric, axial and radial strain against vertical effective stress (Figures 4.1b and 4.2b)
- Volumetric, axial and radial strain against radial effective stress (Figures 4.1c and 4.2c)

For the crown stress path the vertical stress is decreased and the radial stress increased whereas for the springline the converse occurs. However, it can be seen from Figure 2.1a that since the slopes of the two stress paths are very similar then the ratio of the applied stress increments is very similar. For the crown stress path the increase in radial stress is 2.5 times the decrease in vertical stress and for the springline the decrease in radial stress is 3.7 times the increase in vertical stress.

Consequently the data are seen to be consistent in that for an increase in radial stress of 1 MPa for an element at the crown, and a corresponding decrease in radial stress for an element

at the springline, the expected swelling strains (positive for the crown and negative for the springline) will be about the same at 1.7 milli-strain, refer to Figure 4.1c. In general the swelling data associated for the springline are seen to mirror the data for the crown.

At the springline the vertical stress remains significant until failure, and consequently swelling normal to the bedding is repressed. This is indicated in Figure 4.1 where radial strains equal to about twice the axial strains are shown. At the crown the vertical stress is reduced due to the excavation. Initially similar vertical and radial strains are recorded, but as the vertical stress continues to reduce, the axial strain increases in comparison to the radial strain due to the disproportionate reduction in relative vertical and radial confining stresses.

It is apparent from Figure 4.1 that for the stress paths investigated, the swelling strains likely to occur in the field as the result of the unloading process will be very small. This is consistent with the data from the one-dimensional swelling tests described in the following section, where at similar stress levels, swelling strains are modest.

4.4 Triaxial Swelling Tests - Conclusions

The data presented here attempts to replicate the swelling strains associated with the most likely in situ stress paths experienced by the Molasse during the excavation of the cavern. The stress paths applied represented elements located at the crown and springline of the cavern. At the springline the vertical stress remains significant until failure, and consequently swelling normal to the bedding is repressed.

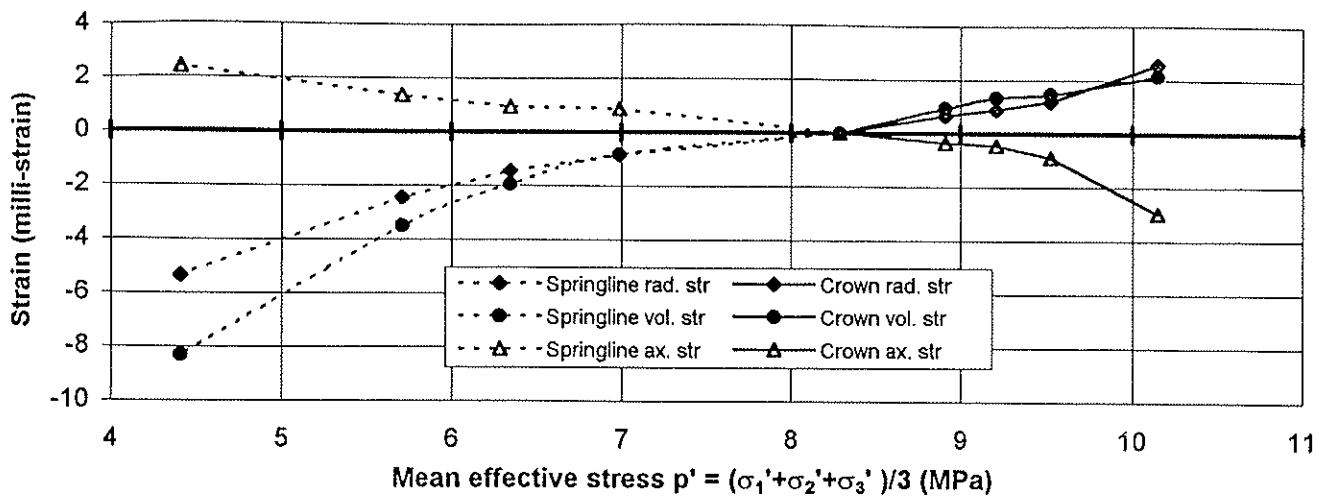
At the crown, the excavation initially results in vertical and radial strains of similar magnitude but as the vertical stress continued to reduce the radial strain decreases and the vertical strain continues to increase.

At both the crown and springline locations represented in the tests, the magnitude of the measured strains was small, and indicates that at the stress levels likely to be experienced during the excavation of the cavern the swelling strains may not be significant.

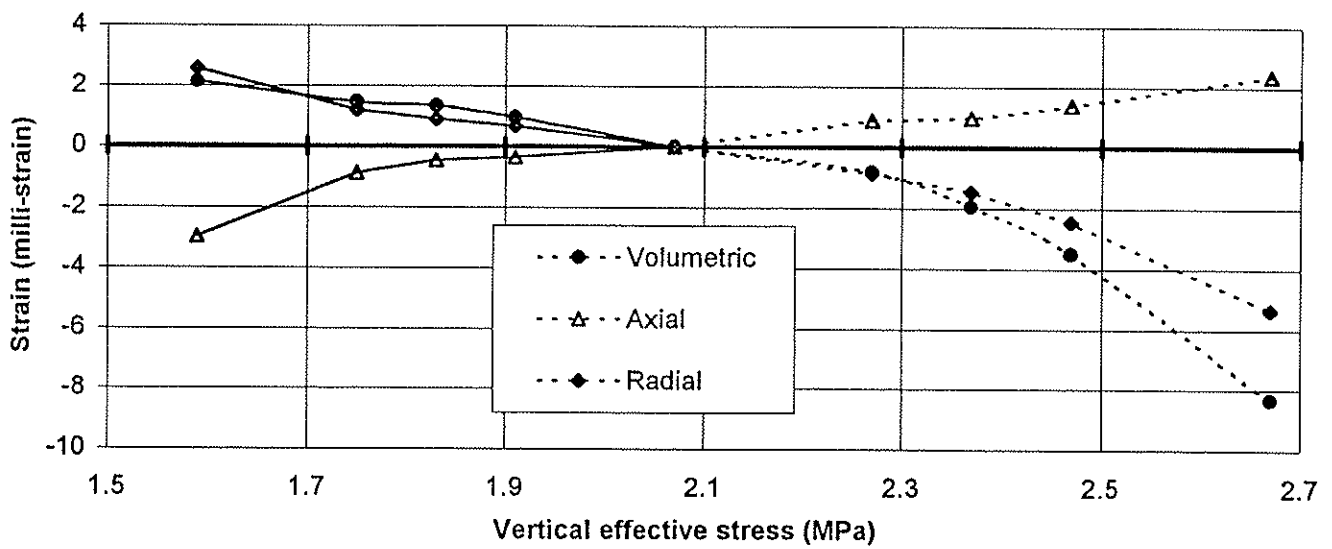
It should be noted that the largest swelling strains would be expected to occur at the floor level of the cavern where the greatest degree of vertical unloading occurs.

Table 7: Summary of triaxial swelling tests

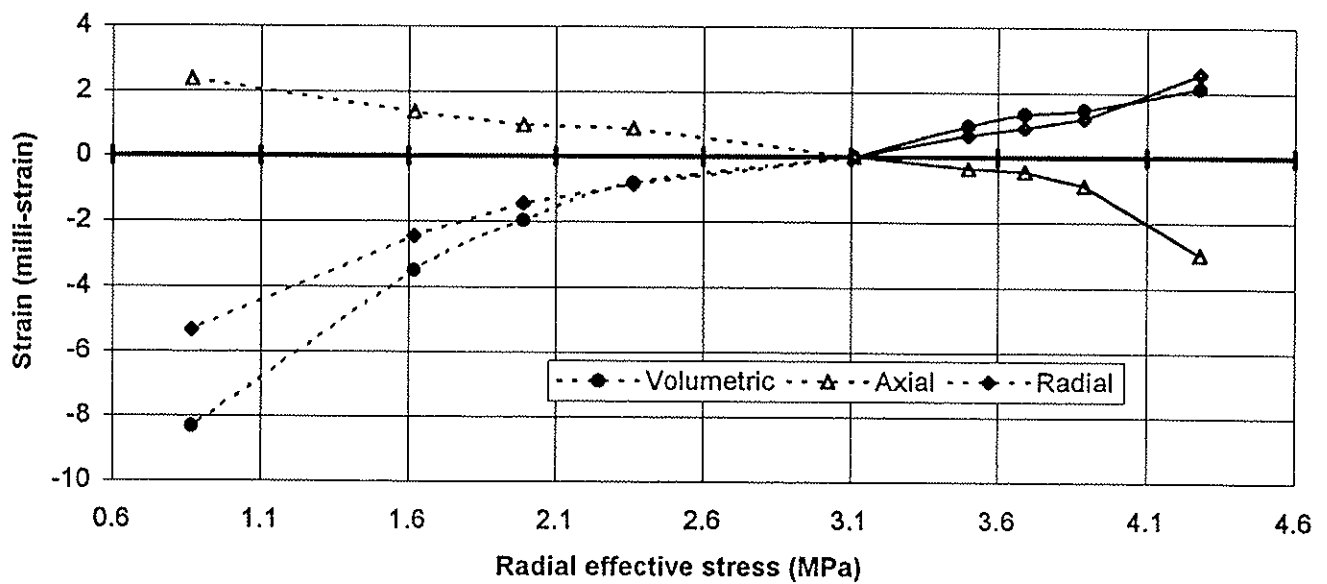
Sample	Moisture content (%)	Effective axial stress (MPa)	Effective lateral stress (MPa)	Cumulative strains (comp.+ve)			Notes	
				Axial strain (mstr)	Lateral strain (mstr)	Vol. strain (mstr)		
SLHC 8117 Crown stress path	8.42	0	0	0	0	0	Initial conditions	
	-----	1.57	2.35	0.985	1.559	4.103	Onset of consolidation stage 1	
	-----			3.059	3.531	10.121	End of consolidation stage 1	
	-----	1.57	2.35	3.059	3.531	10.121	Onset of swelling stage	
	-----			0.503	1.709	3.921	End of swelling stage	
	-----	1.04	3.63	-1.705	3.000	4.295	Onset of consolidation stage 2	
Blk Density 2249 (kg/m3)	-----			-2.823	4.186	5.549	End of consolidation stage 2	
	11.22	0.52	4.91	-----	-----	-----	Sample failure at onset of consolidation stage 3	
SLHC 8219 Crown stress path	8.87	0	0	0	0	0	Initial conditions	
	-----	1.62	2.43	0.831	1.380	3.591	Onset of consolidation stage 1	
	-----			3.476	3.230	9.936	End of consolidation stage 1	
	-----	1.62	2.43	3.476	3.230	9.936	Onset of swelling stage	
	-----			0.764	1.611	3.986	End of swelling stage	
	-----	1.35	3.09	0.156	3.924	8.004	Onset of consolidation stage 2	
	-----			-0.086	4.524	8.962	End of consolidation stage 2	
	-----	0.81	4.41	-1.861	5.668	9.475	Onset of consolidation stage 3	
Blk Density 2249 (kg/m3)	8.94			-2.864	6.709	10.554	Sample failure during consolidation stage 3	
SLHC 8243a Springline	9.62	0	0	0	0	0	Initial conditions	
	-----	2.07	3.11	0.274	6.919	14.112	Onset of consolidation stage 1	
	-----			1.498	8.702	18.902	End of consolidation stage 1	
	-----	2.07	3.11	1.498	8.702	18.902	Onset of swelling stage	
	-----			1.228	8.555	18.338	End of swelling stage	
	-----	2.27	2.36	1.927	8.080	18.087	Onset of consolidation stage 2	
	-----			2.102	7.708	17.518	End of consolidation stage 2	
	-----	2.37	1.99	2.162	7.539	17.240	Onset of consolidation stage 3	
	-----			2.186	7.102	16.390	End of consolidation stage 3	
	-----	2.47	1.62	2.507	6.832	16.171	Onset of consolidation stage 4	
	-----			2.602	6.118	14.838	End of consolidation stage 4	
	-----	2.67	0.87	3.296	5.413	14.122	Onset of consolidation stage 5	
Blk Density 2229 (kg/m3)	10.58			3.597	3.211	10.019	End of consolidation stage 5	
SLHC 8243b Crown	9.62	0	0	0	0	0	Initial conditions	
	-----	2.07	3.11	1.091	8.180	17.451	Onset of consolidation stage 1	
	-----			2.125	9.298	20.721	End of consolidation stage 1	
	-----	1.91	3.50	2.125	9.298	20.721	Onset of swelling stage	
	-----			2.035	9.327	20.689	End of swelling stage	
	-----	1.91	3.50	1.804	9.495	20.794	Onset of consolidation stage 2	
	-----			1.691	9.993	21.677	End of consolidation stage 2	
	-----	1.83	3.69	1.626	10.046	21.718	Onset of consolidation stage 3	
	-----			1.588	10.237	22.062	End of consolidation stage 3	
	-----	1.75	3.89	1.490	10.297	22.084	Onset of consolidation stage 4	
	-----			1.155	10.521	22.197	End of consolidation stage 4	
	-----	1.59	4.28	0.761	10.695	22.151	Onset of consolidation stage 5	
	Blk Density 2230 (kg/m3)	10.85			-0.936	11.896	22.856	End of consolidation stage 5



a



b



c

GIBB



SGI INGENIERIE



CERN - LHC PROJECT - POINT 5

RESULTS FROM TRIAXIAL SWELLING TESTS

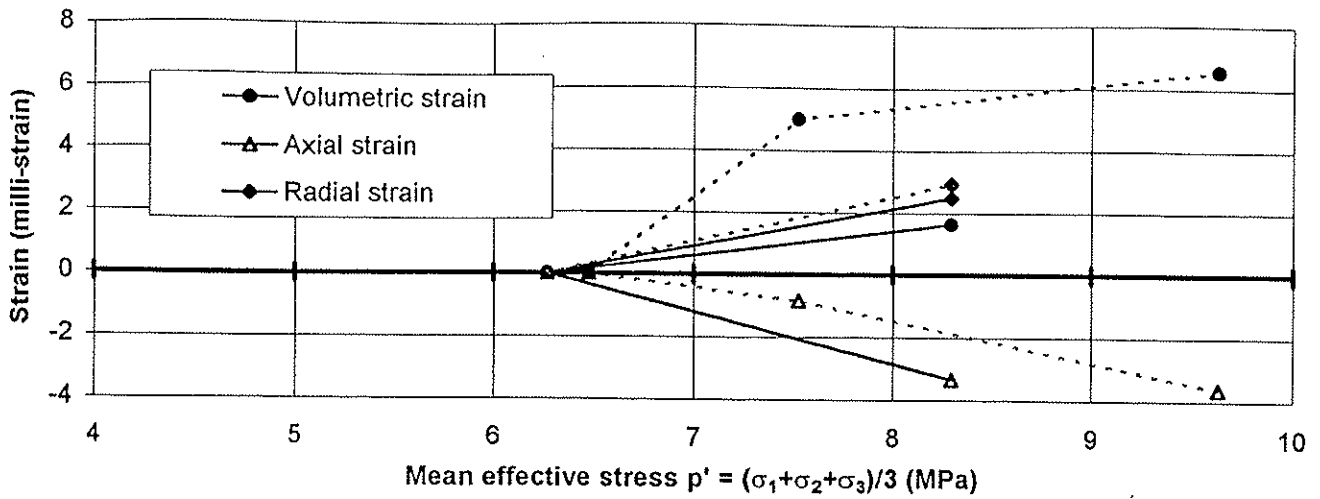
J96107

Date

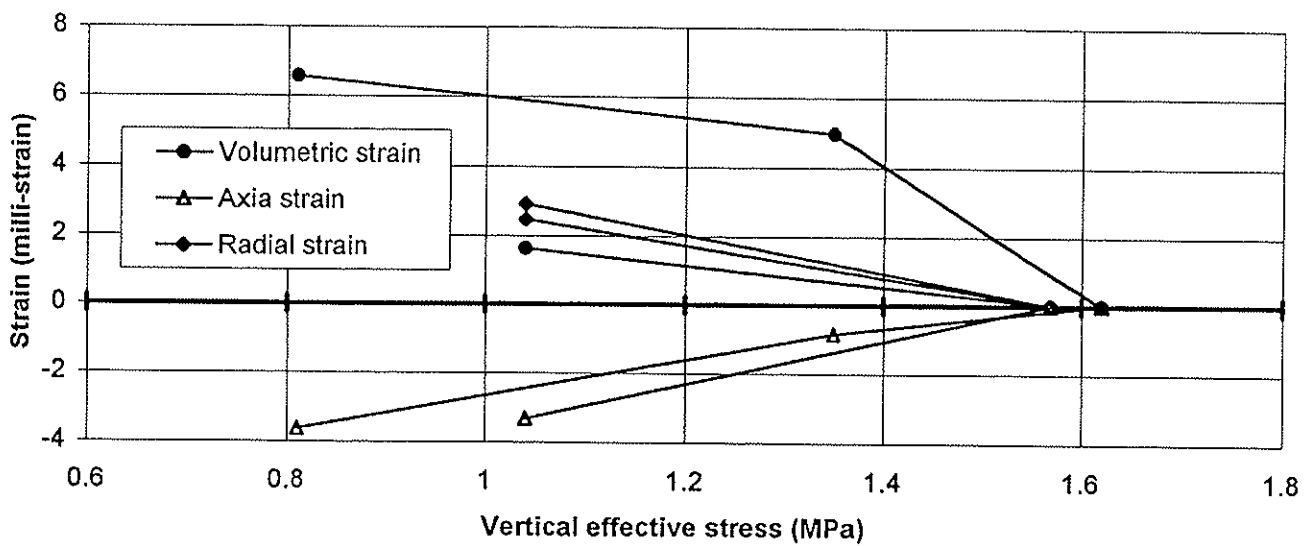
August
1997

Figure

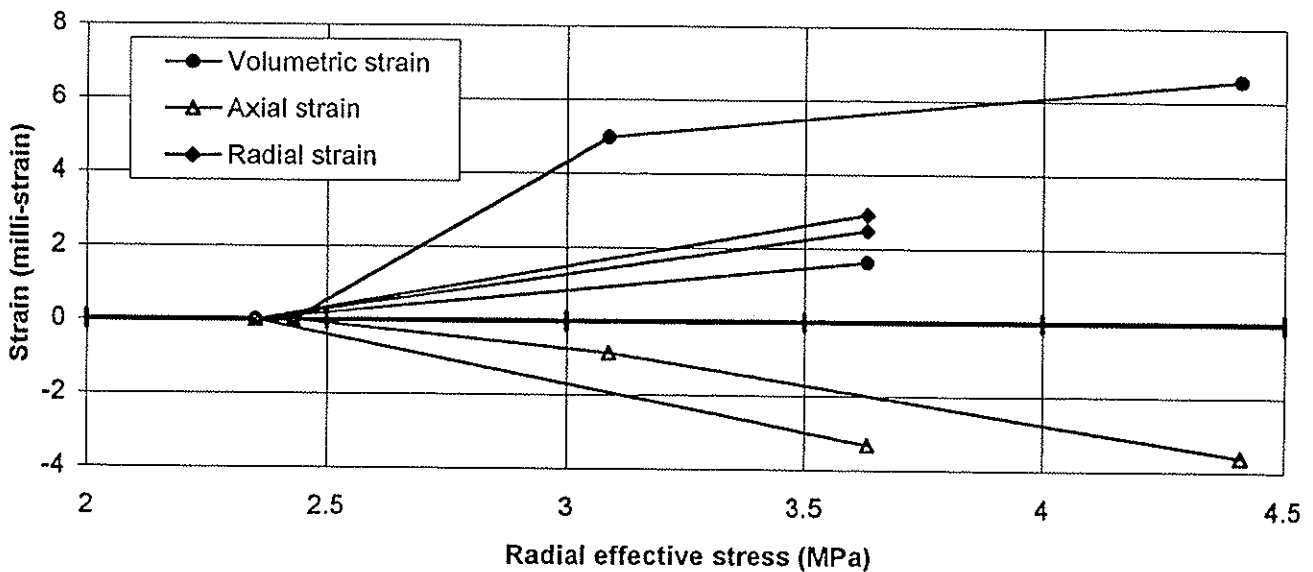
4.1



a



b



c

GIBB



SGI INGENIERIE

CERN - LHC PROJECT - POINT 5

RESULTS FROM TRIAXIAL SWELLING TESTS

J96107

Date
August
1997

Figure
4.2

5 MINERALOGICAL ANALYSES

5.1 Introduction

A series of x-ray diffraction (XRD) tests was performed on twelve samples of marl and marl grumeleuse to determine their mineralogical compositions. The work was carried out by the Centre National de la Recherche Scientifique, Strasbourg, and the results are tabulated below.

Table 8: Results of X-Ray Diffraction Analyses (Non-clay minerals)

Sample No.	Lithology	Quartz %	Plagioclase Feldspar %	Potassium -Feldspars %	Calcite %	Ankerite - Dolomite %	Pyrite %	Clay Fraction %
8153	mg	23	4		16	4	Tr	53
8175	m	22	3		18	10	Tr	47
8181	m	21	3	2	14	13	Tr	47
8191	m	24	3		32	8	Tr	33
8193	mg	25	3		11	3		58
8248	mg	33	4		3	3	Tr	57
8276	mg	25	4		18	6	Tr	49
8277	mg	27	4		10	3		56
8283A	m	30	4	3	26	3	Tr	34
8285	mg	33	5		2			60
8286	mg	29	7	4				60
8288	m	25	4		15	12	Tr	44

Notes: m - marl, mg - marl grumeleuse, Tr - trace

Table 9: Results of X-Ray Diffraction Analyses (Clay minerals)

Sample No.	Lithology	Clay Fraction	Illite		Chlorite		10-14 Smectite	
			% of clay fraction	% of rock	% of clay fraction	% of rock	% of clay fraction	% of rock
8153	mg	53	42	22.26	24	12.72	34	18.02
8175	m	47	40	18.8	26	12.22	34	15.98
8181	m	47	40	18.8	23	10.81	37	17.39
8191	m	33	38	12.54	27	8.91	35	11.55
8193	mg	58	38	22.04	30	17.4	32	18.56
8248	mg	57	46	26.22	29	16.53	24	13.68
8276	mg	49	43	21.07	20	9.8	37	18.13
8277	mg	56	43	24.08	21	11.76	36	20.16
8283A	m	34	41	13.94	23	7.82	36	12.24
8285	mg	60	52	31.2	16	9.6	32	19.2
8286	mg	60	n/a	n/a	n/a	n/a	n/a	n/a
8288	m	44	44	19.36	18	7.92	38	16.72

Notes: m - marl, mg - marl grumeleuse, Tr - trace, n/a not analysed

The results of these analyses are generally in agreement with previous analyses carried out at CERN. The following summary observations may be made:

- The clay fraction of the samples varies between 33 and 60% with the remainder of the samples comprising quartz, feldspars, carbonate minerals (calcite and ankerite-dolomite) and traces of pyrite.
- Swelling-prone clay minerals (denoted 10-14 Smectite) vary in abundance between 11 and 20% of the whole rock, and generally comprise approximately one third of the clay fraction.
- In general, marl grumeleuse samples show the highest clay fractions.

A triangular diagram showing the relative abundances of clay minerals, carbonates and quartz/feldspars is shown on Figure 5.1. The figure includes data from previous investigations at CERN, and data from similar rock types from Italy and the NAGRA investigations in Switzerland. The diagram also gives indications of swelling potential. It can be seen that the data from the additional investigations are consistent with previous CERN data, indicating 'fair' to 'high' swelling potential. The marl grumeleuse data show the highest swelling potential, due to the higher clay contents. However, there are likely to be other controls on swelling behaviour which are unrelated to mineralogy, and so Figure 5.1 may be used only as a broad indication of swelling potential.

5.2 Correlations of Mineralogy with Swelling Index Tests

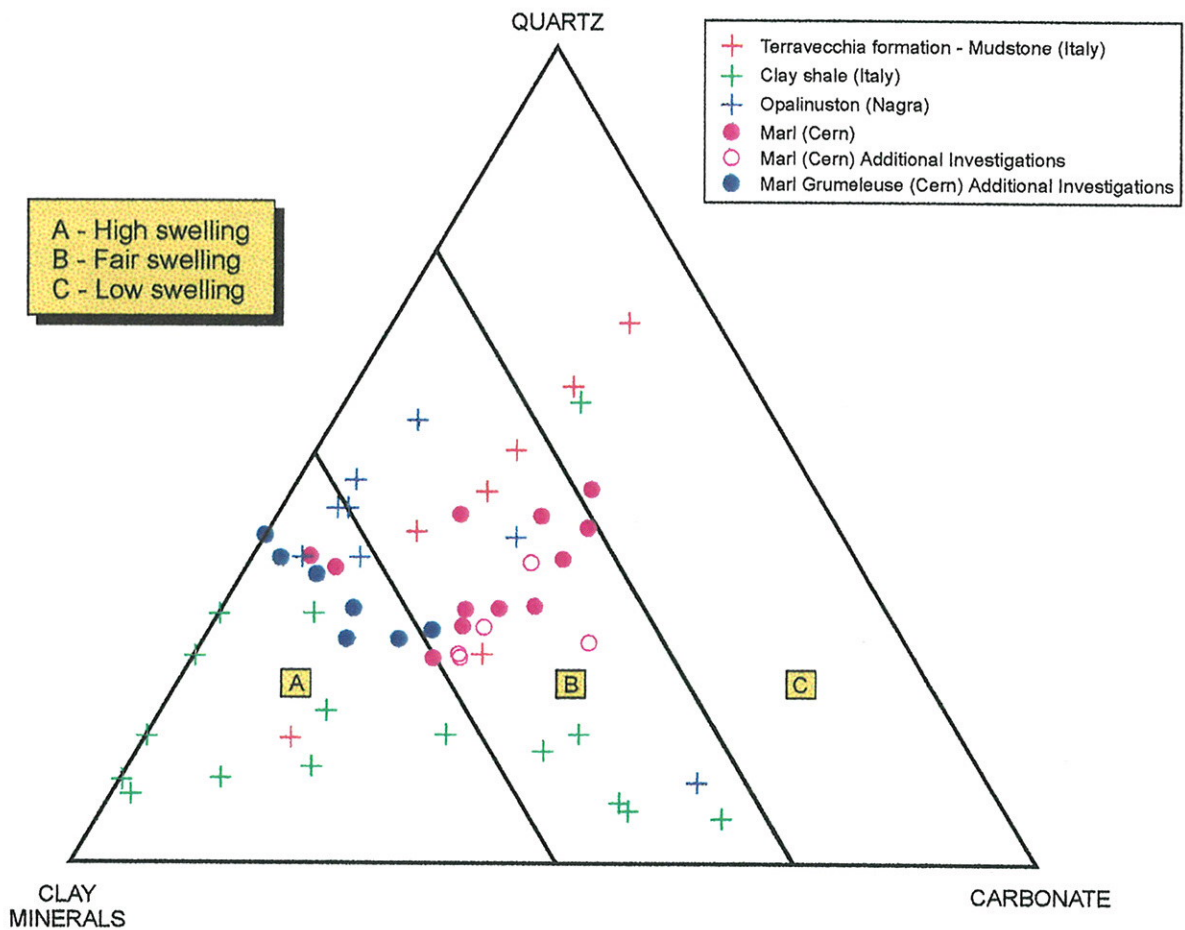
Swelling Index tests are described in detail in Section 6. It is reasonable to expect correlations between the swelling clay mineralogy and the observed swelling behaviour of marl samples. The following summary observations of the test results may be made:



- Correlations between swelling clay content and observed swelling behaviour are variable. This is due partly to the limited sample size, and also to the inherent limitations of the x-ray diffraction analyses carried out. Determinations of the percentages of clay minerals are considered to be more indicative than quantitative, and hence even small errors can result in significant scatter of the data, and variable correlations with other datasets.
- Notwithstanding the above, it can be seen from Figure 5.2a that there is a reasonable correlation between swelling clay content and total clay content, indicating a reasonably consistent clay mineralogy. The swelling clay minerals form approximately one third of the total clay fraction, equating to some 10% to 20% of the rock.
- A fair correlation is shown on Figure 5.2b between swelling clay content and axial swelling pressure, with generally higher swelling pressures being shown by samples with higher swelling clay contents. Two samples shown anomalously high swelling pressures approaching 600 kPa (one of which has a very high clay content of almost 60%), but the remaining data are reasonably consistent with swelling pressures of 250 - 400 kPa at swelling clay contents of 18 - 20% of the rock.
- A better correlation can be seen in Figure 5.2c between swelling clay content and axial swelling strain, with higher axial swelling strains being shown by samples with higher swelling clay contents, as would be expected. Maximum swelling strains range between 20 - 30% at swelling clay contents of 18% to 20% of the rock.

5.3 Mineralogical Analyses - Conclusions

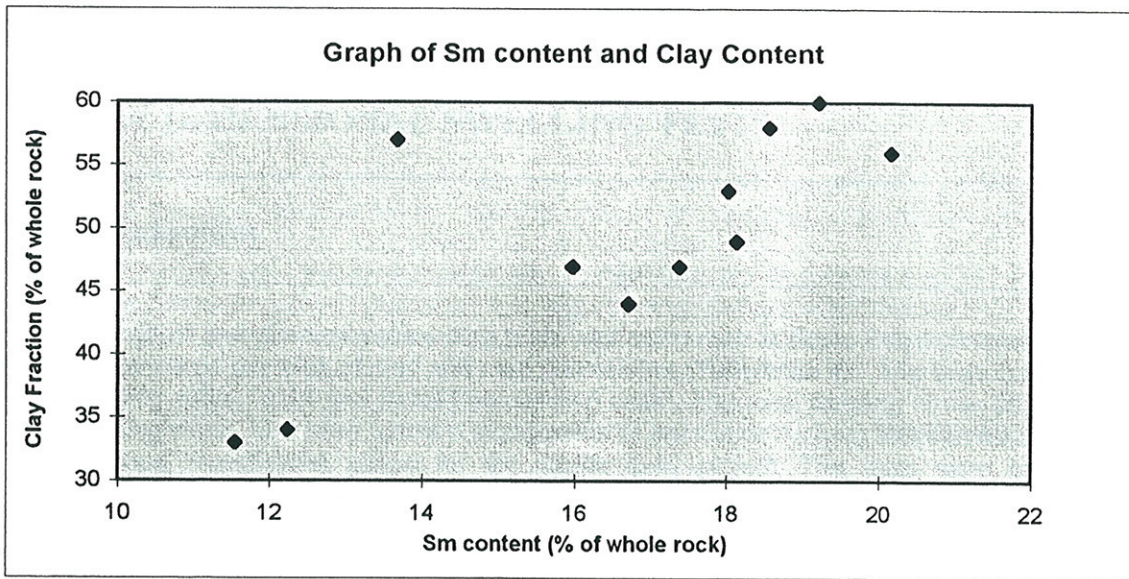
In summary, the following conclusions may be drawn:

- Mineralogical analyses confirm that marls have potential for swelling. A broad comparison with similar marl materials from elsewhere indicates that the potential for swelling is 'fair' to 'high'.
- Marl grumeleuse samples show the highest clay content and hence show the highest swelling potential based upon broad mineralogical indicators alone.
- Correlations between swelling clay content and axial swelling pressure and strain (normal to bedding lamination) are to be expected, and are shown by the data. Higher swelling pressures and swelling strains are shown by samples with high swelling clay contents.

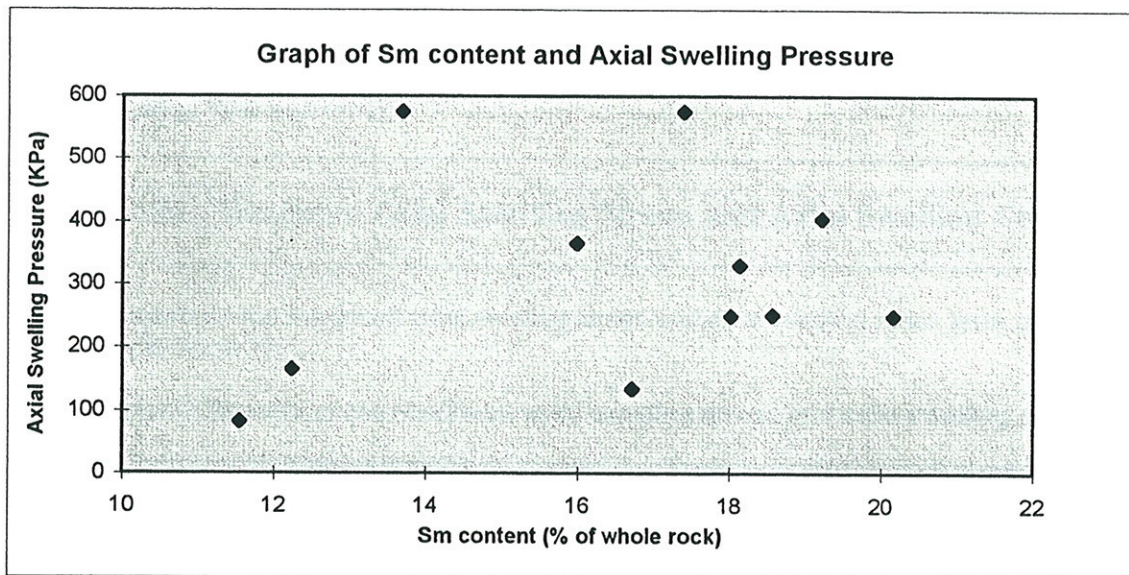


GIBB  SGI INGENIERIE		CERN - LHC PROJECT- POINT 5		J96107C	
		COMPOSITION AND INFERRED SWELLING POTENTIAL OF MOLASSE MARLS IN COMPARISON WITH OTHER MARL FORMATIONS		Date NOVEMBER 1997	Figure 5.1

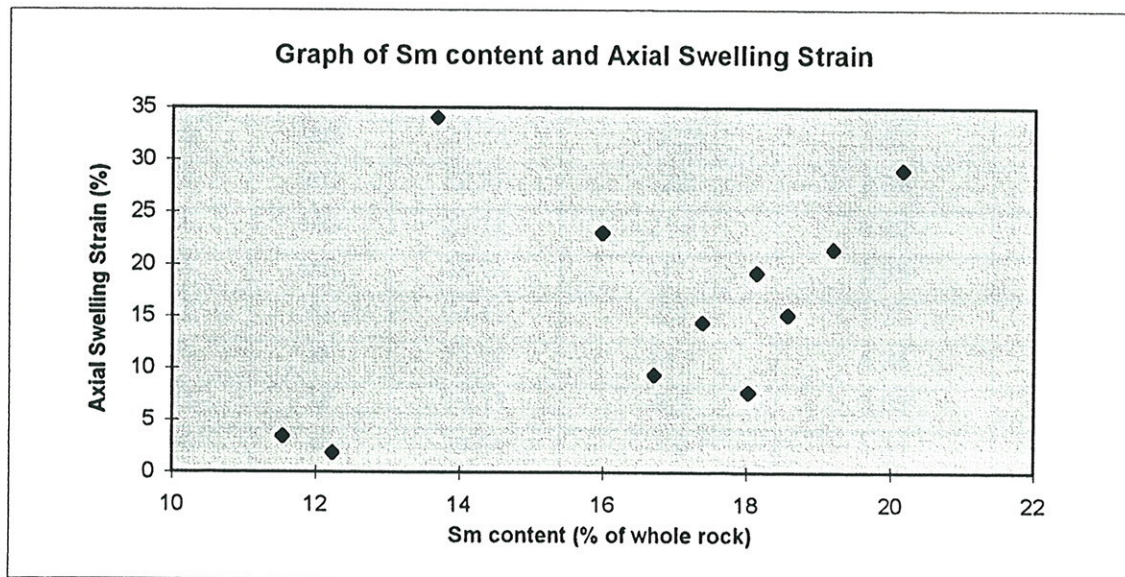
(a)



(b)



(c)



GIBB



CERN - LHC PROJECT - POINT 5

J96107



CORRELATIONS OF SWELLING MINERAL
CONTENT WITH SWELLING BEHAVIOUR

Date
November
1997

Figure
5.2

6 ONE DIMENSIONAL SWELLING TESTS

6.1 Introduction

A range of one-dimensional swelling tests was performed at Ecole Polytechnique Federale de Lausanne on samples of marl and marl grumeleuse (Reference 4). The tests comprised axial swelling stress, axial and radial free swelling strain, and axial swelling stress as a function of swelling strain. The latter test is a modification of the Huder-Amberg test carried out during the previous investigation phase for the CERN LHC project. The tests were carried out in accordance with the ISRM Suggested Methods (Reference 5).

The maximum axial swelling stress and free swelling strain tests are index tests intended for rapid assessment of swelling potential, whilst determination of axial swelling stress as a function of swelling strain allows a more rigorous assessment of swelling behaviour, albeit only in one dimension. Axial swelling stress and swelling strain tests were carried out on the same samples as XRD determinations in order to investigate correlations of swelling behaviour with mineralogy (see Section 5).

6.2 Results - Maximum Axial Swelling Stress and Axial Swelling Strain Tests

The results of the maximum axial swelling stress and axial swelling strain tests are presented below in Table 10.

Table 10: Results of the maximum axial swelling stress and axial swelling strain tests

Sample	Lithology	Bulk density kN/m ³	Free axial swelling strain (%)	Free radial swelling strain (%)	Free axial swelling pressure (kPa)
8153	MG	23.19	-7.75	1.25	250
8193	MG	22.93	-15.2	2.43	252
8248	MG	23.56	-34	1.56	575
8276	MG	23.74	-19.25	1.52	330
8277	MG	22.97	-29	2.09	250
8285	MG	23.72	-21.5	0.92	405
8286	MG	23.74	-17	0.55	188
8175	M	24.42	-23	1.22	365
8181	M	23.73	-14.5	4.24	575
8191	M	25.11	-3.5	3.03	83
8283	M	24.61	-1.9	1.31	165
8288	M	23.57	-9.4	0.17	135

The following summary observations of the test results may be made:

- The maximum axial swelling stresses lie in the range 75 to 600 kPa with most results (eight) in the range 150 to 400 kPa.
- Free axial swelling strain results range up to 34% with six results in the range 14 to 24%.

- Free radial swelling strain results range up to 4.3% although most are less than 2.5%.

These results confirm that swelling behaviour is likely to be significant normal to bedding but much less significant parallel to bedding. Very high swelling pressures and strains such as those associated with evaporite minerals (e.g. anhydrite) are not indicated. The general swelling behaviour is consistent with the mineralogical composition of the samples determined by the XRD analyses. Correlations between the swelling test data and the mineralogical data are described in Section 5 above.

6.3 Results - Axial Swelling Stress as a Function of Swelling Strain Tests

Axial swelling stress as a function of swelling strain tests have been conducted previously for CERN using the Huder-Amberg technique. For the current investigation, the general Huder-Amberg test procedure was modified to be in accordance with the ISRM Suggested Method (Reference 5). For ease of reference, the text below refers to Huder-Amberg tests and ISRM tests for these two variations of the general test procedure. All tests were carried out normal to bedding.

The Huder-Amberg test procedure includes an unreload-reload loop during the dry loading stage to permit determination of elastic unloading strains and allow the subsequent calculation of swelling strains. However, such elastic unloading behaviour may be different for dry (or partially saturated) and saturated conditions. To avoid this problem, the ISRM procedure requires that elastic unloading strains are determined directly from the saturated unloading stage as it is straightforward to separate elastic strains and swelling strains. The same data assessment procedure can be applied to the Huder-Amberg tests to yield comparable results. The only possible effects on the data therefore result from the additional unload-reload loop, and possible damage to the sample fabric. However, such effects have not been assessed.

Figure 6.1 shows the data from free swell, swell pressure and ISRM swelling pressure-swelling strain tests plotted in terms of swelling pressure against swelling strain for both marl and marl grumeleuse. For both materials it can be noted that higher swelling strains and lower swelling pressures were measured in the free swell and swelling strain tests than were measured in the ISRM and Huder-Amberg tests. For both materials it is evident that the swelling strain is significant for swelling pressures less than 150 kPa but reduces rapidly at greater pressures. The mean and mean plus one standard deviation lines are also plotted. The subdivision of lithology was carried out by reference to the borehole logs at the sample locations, as the test data sheets generally did not identify where a grumeleuse texture was evident in the samples. The differences in the test results produced by different test methods may be due to the different load paths experienced by the samples. The free swell test is performed on samples with only a nominal axial confinement (25 kPa), and hence is not representative of in situ conditions in the ground. As stated previously, this test is merely an index test to provide an indication of swelling potential.

Figure 6.2 shows the Huder-Amberg test results from the original LHC investigations at Point One and Point Five. A single Huder-Amberg test result shows swelling significantly in excess of all other samples. This was a sample of weak laminated marl recovered from borehole SLHC22 at a depth of 87.1 m. The sample showed a very high initial moisture content, approximately double that recorded for all other samples. This sample is not therefore considered to be representative. The graph also shows the Phase Two Design Line, the mean line and the mean plus one standard deviation. The calculations for the latter two lines did not include the data from the outlying test described above.

Figure 6.3 presents the mean lines and mean plus one standard deviation lines for both datasets. This illustrates the significantly higher mean and larger range of scatter for the

additional test data compared with the original test data. This may be due to natural variability of the material, and also to a slight difference in test procedure. In the Huder-Amberg tests, each 'dry' loading increment was limited in duration to 15 minutes, whilst in the ISRM tests, each increment was maintained until no further deformation was recorded. This may result in the expulsion of more pore water using the ISRM procedure, possibly giving higher swelling strains on resaturation.

Figure 6.4 shows all the Huder-Amberg and ISRM test data plotted together, and differentiated by test type and lithology. The range of swelling strains for a given swelling pressure is generally greater for the marl grumeleuse than for the marls, and the marl grumeleuse generally show slightly higher swelling strains than the marls. This is consistent with expectations from mineralogical tests as noted in Section 5. However, the scatter of data is such that it cannot be concluded that a sample of marl grumeleuse will necessarily exhibit significantly greater swelling behaviour than one of marl. This is consistent with previous assessments of the data (Reference 6).

The figure also shows the design swelling curve used in Phase Two design (presented in Reference 7) for swelling normal to bedding (denoted 'Phase Two Design Curve'). This can be seen to under-predict the swelling data from some of the tests. Also shown on Figure 6.4 is the curve representing the mean of all the data (excluding the sample described above). This is almost coincident with the Phase Two Design Curve (which was derived from analysis of all the data). A third curve is presented which shows the mean of the data plus one standard deviation (excluding the outlying data). This curve may be smoothed and slightly adjusted to give a curve which bounds most of the data and could reasonably be accepted as representing 'worst case' swelling behaviour.

No additional data are available concerning swelling stress as a function of swelling strain parallel to the bedding, but the assumption that it would be significantly less than the swelling normal to the bedding is considered reasonable, based upon the index test results described in Section 6.2. In Phase Two, it was assumed that swelling strains parallel to bedding would be approximately 60% of the strains normal to bedding, and this is considered to be a reasonable and conservative design assumption for Phase 3 design.

The assumed curves do not represent the ultimate swelling strains generated at swelling pressures below 100 kPa as all tests were still showing ongoing swelling on termination of the final load decrement.

A direct comparison between the triaxial swelling data and the one dimensional swelling data is not feasible since the stress paths for the two types of tests were different and the ISRM tests are not generally reliable for the measurement of very small strains. However, the general observation is made that, at higher stress levels, the triaxial swelling data and the one dimensional swelling data both indicate that only small swelling strains are likely.

6.4 Application of Results in Design

6.4.1 Application of One-Dimensional Test Results

Various models have been proposed for excavation design in swelling rock. These range from simple total stress models to complex coupled hydro-mechanical models. A brief review of these models is presented in Reference 8. The models incorporate 'swelling laws' to characterise the behaviour of the rock, and such laws also vary in complexity. The basic swelling law which relates swelling strain (change in volume) with decreases in swelling pressure (applied stress) may be obtained directly from oedometer tests (Reference 5) such as have been described in Section 6.3 above. The ISRM design and analysis procedures

(Reference 8) do not discuss any scaling required when applying laboratory measurements to design methods to predict in situ conditions. However, the ISRM suggested method for determining axial strain as a function of axial stress (Reference 5) does suggest that the unloading procedure used in the test is expected to produce lower bound swelling stresses for a particular swelling strain, and that the method "is appropriate for determining heave resulting from unloading". This should be considered when selecting stress-strain relationships for design. The analysis method of Einstein et al (Reference 9) involves the use of correction factors to extend the results of one dimensional oedometer tests to a three dimensional analytical procedure.

6.4.2 Appropriate Design Methods

One of the principal observations regarding the swelling behaviour of clay-bearing lithologies around underground excavations is that swelling is invariably observed only in the excavation floor, as heave, and rarely in the sidewalls or crown. This observation is believed to result from the greater availability of free water in the invert due to drainage and flow under gravity, compared to the crown and sidewalls. Stress analysis-based design methods predict swelling not only in the invert, but also in the crown and sidewalls as they assume that free water is available everywhere for the swelling process. This is at odds with the generally observed rock mass swelling behaviour.

A design method, involving a coupled hydro-mechanical constitutive model, has been developed which more faithfully simulates invert swelling behaviour (Reference 10). The hydraulic boundary conditions for this model assume the presence of free water on the tunnel floor, or in the loosened zone beneath the tunnel floor. This results from seepage of water towards the excavation, driven by the difference in pressure head from hydrostatic within the rock mass, to atmospheric pressure around the invert of the excavation. This is considered to be equivalent to the development of a phreatic surface at approximately the same level as the tunnel invert (Reference 10). In order for swelling to occur in the sidewalls and crown, the conceptual model requires water to move from the invert upwards by seepage. Such movement will be limited and hence results in only very minor swelling. The boundary conditions for the conceptual model may be compared with the actual ground conditions at the Point Five site.

The principal hydrogeological features of the site are;

- The molasse is considered to be an aquiclude, with very low matrix permeability.
- In situ testing has indicated that there is unlikely to be a hydraulically-connected natural fracture network.
- The molasse is overlain by the principal aquifer of the area, comprising sands and gravels (moraine) with high storage and transmissivity characteristics.
- The proposed caverns lie within a short vertical distance of the moraine / molasse interface (approximately one cavern span), and deformation of the cavern crown zone may lead to induced fracturing of the rock, increased rock mass permeability and connection to hydraulic recharge boundary.

It can be seen therefore, that if hydraulic connection to the moraine occurs as a result of rock mass deformation in the cavern crown zone, the boundary conditions of the site will differ significantly from those of the above conceptual model. Water may flow downwards around the cavern increasing the potential for swelling in the cavern crown and sidewalls, although this effect is designed to be mitigated by drainage measures in the cavern roof zone.

A stress analysis-based approach, as used in Phase Two, would therefore appear to be appropriate to predict swelling of the cavern crown, sidewalls and invert in the presence of free water.

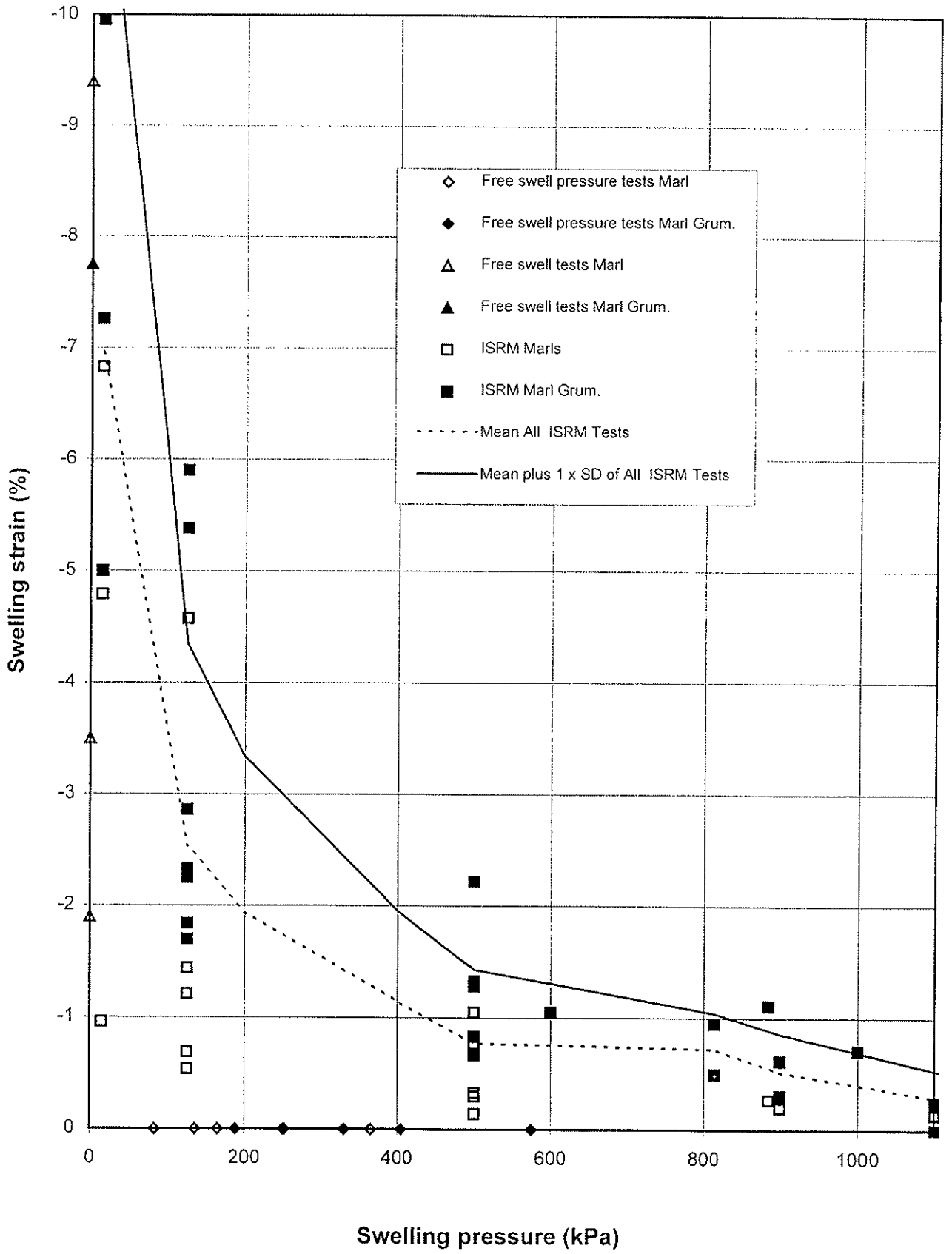
6.5 One Dimensional Swelling Tests - Conclusions and Recommendations

The following conclusions can be drawn from the swelling test programme;

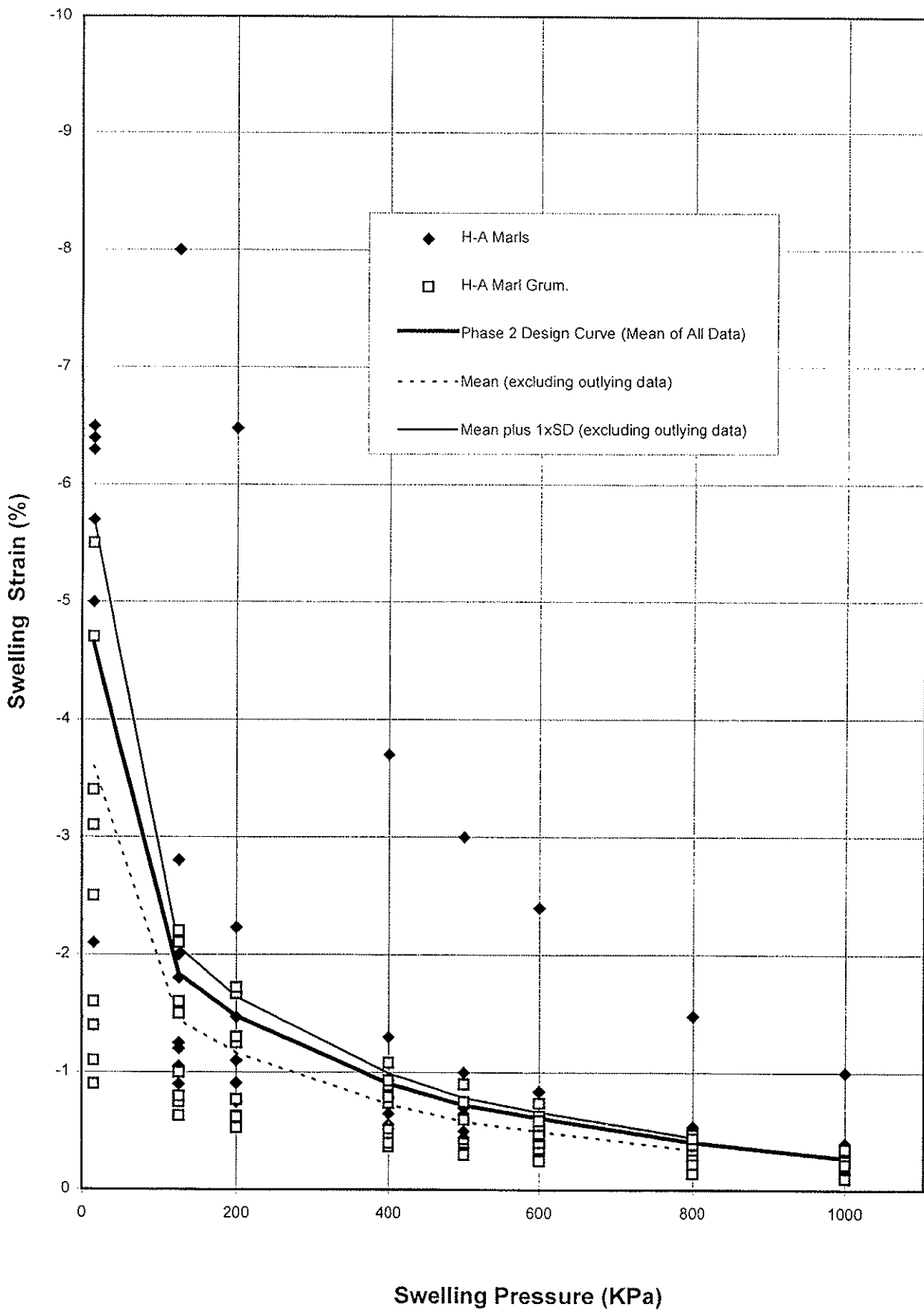
- The swelling characteristics of the marl and marl grumeleuse are very similar and could both be represented by the same design curve.
- The design swelling curve used in Phase Two does not bound all the new data. It is coincident with the mean of all the data and is therefore representative of 'typical' conditions, rather than being a conservative design assumption.
- A new design swelling curve, representing 'worst case' behaviour can be derived from analysis of both datasets combined.
- The swelling curves do not reflect the high swelling strains associated with swelling stresses below 100 kPa.

With reference to the proposed excavations at Point Five and the generally observed behaviour of excavations in swelling-prone rock, the following recommendations may be made;

- For the proposed works at Point Five, a significant hydraulic recharge boundary is located within a short distance above the cavern crown which may make free water available for swelling in the rock mass in the cavern crown and sidewalls, as well as the invert. It is considered necessary to allow for such swelling of the rock mass in the design. In this case, it would be appropriate to adopt the design curves from Figure 6.4 to investigate the swelling behaviour of the ground using a stress analysis-based design method. The Limiting Curve represents an onerous load case taking account of the induced hydraulic regime and the provision of drainage. The Average Swelling Curve should therefore be considered for design as a normal load case whilst the Limiting Curve should be considered as a exceptional load case.
- For the more critical case of the invert, it is recommended that the Limiting Curve is used to represent the swelling behaviour of the ground, as it is likely that free water will occur in the invert.
- For swelling parallel to bedding, the swelling strains shown by the design curves in each case may be reduced by 40%, as for the Phase Two analyses.



p:\project\cern_ph3\reports\tablest\swelldata.xls



GIBB



CERN - LHC PROJECT - POINT 5

J96107

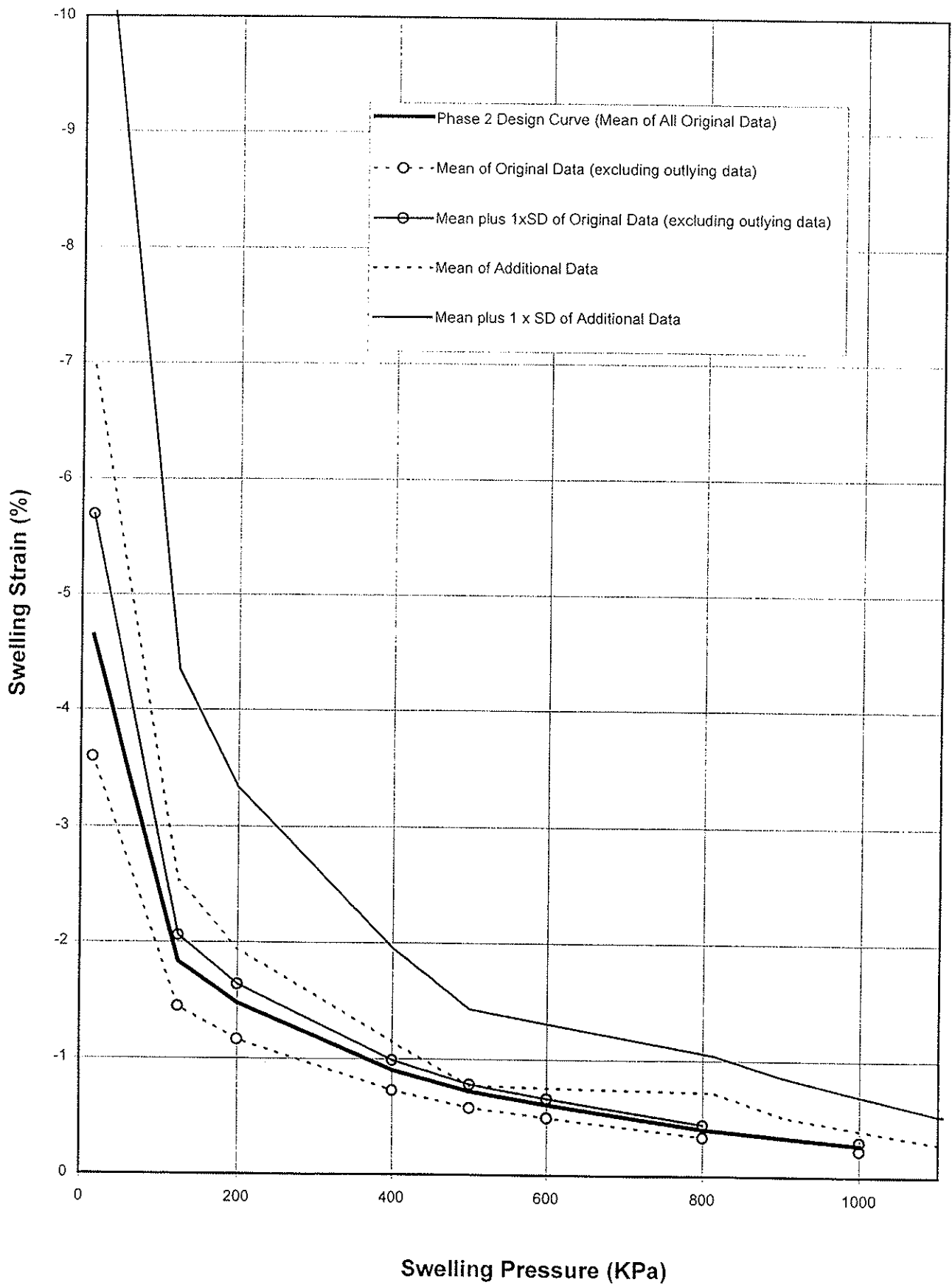


SGI INGENIERIE

1-D SWELLING DATA (NORMAL TO BEDDING)
DATA FROM ORIGINAL INVESTIGATION

Date
November
1997

Figure
6.2



GIBB



CERN - LHC PROJECT - POINT 5

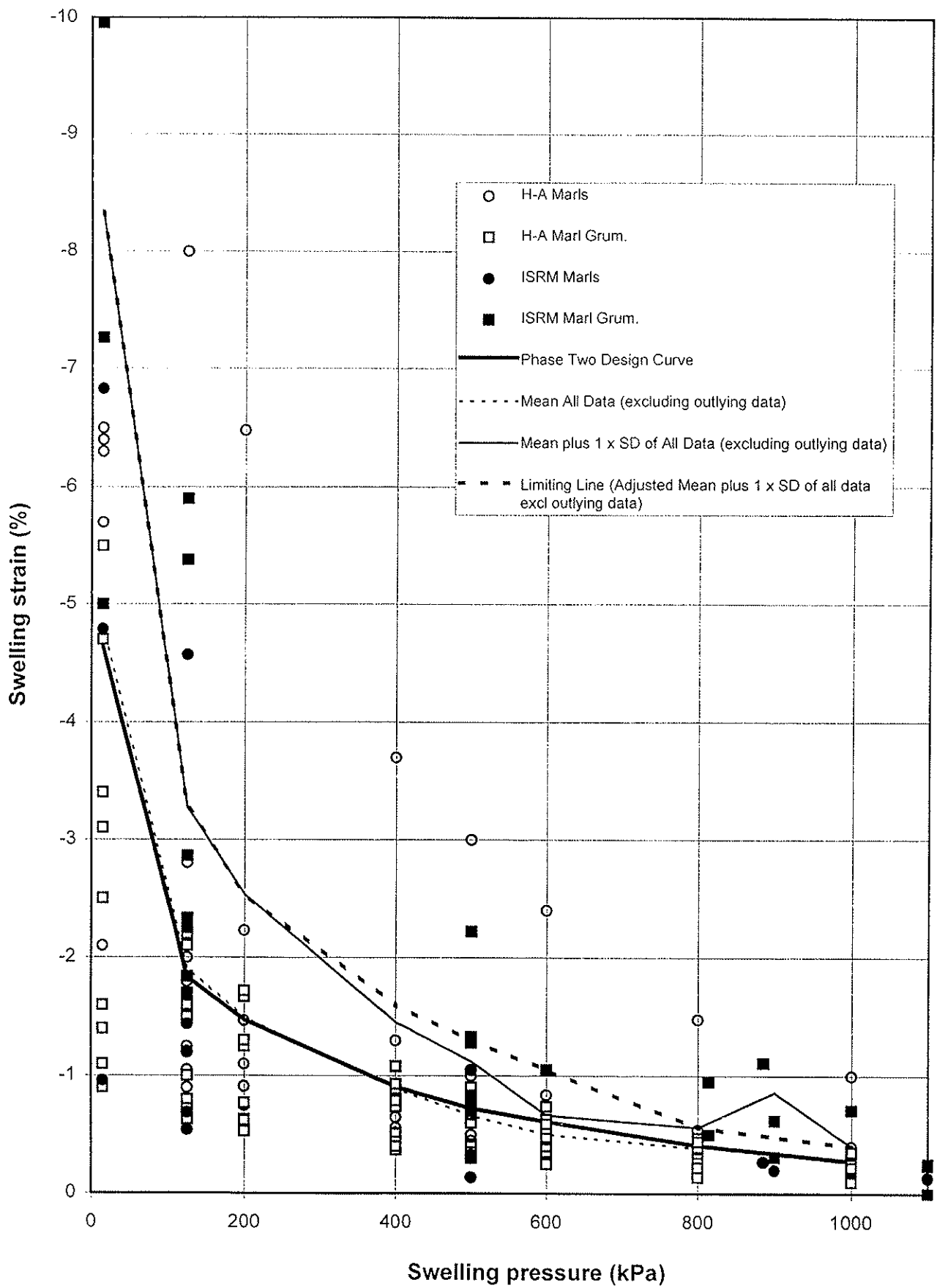
J96107



1-D SWELLING DATA -SUMMARY CURVES

Date
November
1997

Figure
6.3



GIBB



CERN - LHC PROJECT - POINT 5

J96107



SGI INGENIERIE

1-D SWELLING DATA (NORMAL TO BEDDING)
ALL DATA & DESIGN CURVES

Date
November
1997

Figure
6.4

7 CONCLUDING REMARKS

From the tests reported here the following conclusions can be made with reference to the relevant parameters presented in the Design Specification (Reference 7) and reproduced below in Table 11 (For a detailed description of the derivation of creep parameters see Reference 7).

Table 11 Design Parameters

		Initial Condition									
		ρ	σ_c	σ_t	ν	E	K	G	ϕ int	c	
	Abbr.	(g/cm ³)	(MPa)	(MPa)		(MPa)	(MPa)	(MPa)	(°)	(MPa)	
Marl grumeleuse	MG	2.46	5.0	0.5	0.25	1000	1111	370	20.0	0.2	
Marl laminated	ML	2.5	10.0	1.0	0.25	2800	1867	1120	35.0	1.0	
Marl sandy (Transition)	SM	2.50	25.0	2.5	0.20	4000	2667	1600	40.0	1.0	
		Creep 0		Creep 1				Creep 2			
		c_{c0}	E_{c0}	c_{c1}	E_{c1}	K_{c1}	G_{c1}	c_{c2}	E_{c2}	K_{c2}	G_{c2}
	Abbr.	(MPa)	(MPa)	(MPa)	(MPa)	(MPa)	(MPa)	(MPa)	(MPa)	(MPa)	(MPa)
Marl grumeleuse	MG	1.0	1000	0.5	600	667	222	0.0	300	333	111
Marl laminated	ML	1.3	2800	0.8	1700	1133	680	0.2	850	567	340
Marl sandy (Transition)	SM	2.2	4000	1.4	3300	2200	1320	0.5	2800	1867	1120

The design effective strength envelopes (for Initial Conditions) are based on lower bound peak strength parameters. The peak strength data obtained in the current testing programme lies, as expected, above the design effective strength envelope and confirms the adequacy of the design parameters.

The creep tests have provided data against which the assumed magnitude of long term stiffness reduction can be estimated. The 50 and 70 % reduction in deformation modulus used for design (Creep 1 and Creep 2 load cases) have been shown to be consistent with the experimental results.

The one-dimensional swelling tests indicate that the Phase Two design swelling curve shown on Figure 6.3 will under-predict the swelling response of the marls. A modified design curve (Limiting Curve) for swelling normal to the bedding lamination is recommended and presented. For swelling parallel to the bedding, the swelling strains derived from the design curves for swelling normal to bedding should be reduced by 40% (as for the Phase Two analyses).

Both the triaxial and one-dimensional swelling tests indicate that in situ swelling strains are likely to be small at locations where the vertical stress remains relatively high, such as at the

springline, but may be more significant at the floor or crown where a greater degree of vertical unloading occurs.

8 REFERENCES

1. NGI (1997) Triaxial Strength Tests for CERN Report No: 971012-1.
2. ISMES (1997) Triaxial Creep Tests for CERN.
3. Royal School of Mines (1997) Multi-stage consolidated-drained anisotropic triaxial and swelling tests on Marls ex. CERN project. Report No: IC/603-97/4
4. EPFL (1997) One-dimensional swelling tests performed at EPFL.
5. International Society for Rock Mechanics (1989). Suggested methods for laboratory testing of argillaceous swelling rocks. *Int. J. Rock Mech. & Min. Sci.* 26(5) September 1989.
6. GIBB-SGI-Geoconsult Joint Venture (1997). LHC Civil Engineering Consultancy Services. Package 02. Geotechnical Interpretative Report. Document 02/Revision 2. April 1997.
7. GIBB-SGI-Geoconsult Joint Venture (1997). LHC Civil Engineering Consultancy Services. Design Specification Nr. 1 Revision 07, Rock Support - Large Caverns.
8. International Society for Rock Mechanics (1994). Comments and recommendations on design and analysis procedures for structures in argillaceous swelling rock. *Int. J. Rock Mech. & Min. Sci.* 31(5) October 1994.
9. Einstein, H., Bischof, N. and Hofmann, E. 'Verhalten von Stollensohlen in quellendem Mergel', in Grob, H. and Kovari, K. (eds) *Proc. Int. Symp. on Underground Openings*, Lucerne, Swiss Soc. for Soil Mechanics and Foundation Engineering. Zurich 1972, pp296-319.
10. Anagnostou, G. (1993) A Model for Swelling Rock in Tunnelling. *Rock Mech. Rock Engng* 26(4), pp 307-331